

# Controlling factors and implications for travertine and tufa deposition in a volcanic setting

Álvaro Rodríguez-Berriguete <sup>\*</sup>, Ana María Alonso-Zarza

Dpto. Petrología y Geoquímica, Facultad de Ciencias Geológicas, Universidad Complutense de Madrid, José Antonio Nováis 2, 28040 Madrid, Spain  
Instituto de Geociencias (CSIC-UCM), José Antonio Nováis 2, 28040 Madrid, Spain

## ARTICLE INFO

### Article history:

Received 10 October 2018  
Received in revised form 3 December 2018  
Accepted 4 December 2018  
Available online 26 December 2018

Editor: Dr. B. Jones

### Keywords:

Travertine  
Tufa  
Aragonite  
Calcite  
Biofilm  
Inorganic CaCO<sub>3</sub>

## ABSTRACT

This work studies a fossil system of perched and fluvial travertines passing distally to fluvial tufas within a volcanic ravine. Sedimentology, petrology and geochemistry of fossil aragonitic-calcitic travertines and downstream calcitic tufas from the Azuaje volcanic ravine were studied. These spring-related carbonates seem to be formed after the Mid-Holocene climate change, the transition from a monsoon-dominated humid climate to an arid-semiarid climate controlled by trade winds.

The main travertine facies include rafts, dendrites/shrubs, ooids, oncolites and stromatolites among others, whereas tufas are characterised by phytoclasts, oncolites, coated stems, intraclasts and stromatolites.

Facies observed can be (i) microbial-influenced when the microbial growth rate is greater than the precipitation rate and flow energy is not above the threshold value tolerated by microbes, or (ii) inorganic-dominated if the precipitation rate exceeds that of the microbial growth rate and/or flow energy is above the threshold tolerated by microbes.

Travertine facies vary from mostly inorganic to microbially-dominated, whereas tufa facies are mostly microbially-influenced. Observed changes of facies in both travertines and tufas were interpreted as due to changes in environmental conditions from (a) less to more evaporative, (b) less saturated to oversaturated, and (c) high to low energy. Changes in textures, mineralogy, geochemistry and stable isotope composition downstream from travertine to tufa suggest a decrease in the CaCO<sub>3</sub> precipitation rate and an increase in microbial influence from travertines (proximal part of the system) to (distal) tufas.

Our study case illustrates the wide variety of facies and processes operating in spring-related travertine and tufa deposits. The details of arrangement, mineralogy, facies and geochemistry of the deposits were mostly controlled by climate and hydrogeology, although the volcanic setting, provided suitable conditions for spring-carbonate deposition.

© 2018 Elsevier B.V. All rights reserved.

## 1. Introduction

Travertines and tufas are spring-related carbonate deposits which occur in many different climate and geological settings. Groundwaters supersaturated in CaCO<sub>3</sub> are required for sedimentation of spring-related carbonates. The ions needed can be supplied by sedimentary carbonates, volcanic rocks, or also metamorphic rocks forming the aquifer (Özkul et al., 2002; Pentecost, 2005; Capezzuoli et al., 2014; Stefánsson et al., 2016). When the appropriate balance between rainfall and aquifer recharge occurs, supersaturation of groundwaters takes place and spring activity is kept. This balance can depend on climate, lithological composition of the aquifer, and others such as residence times of groundwaters within the aquifer (Custodio, 2004; Pirajno, 2009; Kafri and Yechieli, 2010; Gysi and Stefánsson, 2012).

Although waters saturated in CaCO<sub>3</sub> have been recognised as required for deposition, the role played by microbes in deposition of microbial-related travertine and tufa has been widely discussed, the subject of many recent works (Liu et al., 2006, 2010; Okumura et al., 2011, 2012, 2013; Shiraishi et al., 2018). Spring-related carbonates form under precipitation rates of several mm-cm per year, generally higher than those of most microbial-related carbonates (Pentecost, 2005). In many cases it is the interaction between microbes and inorganic precipitation at high rates, together with the (changing) flow conditions, which leads to travertine and tufa facies (Okumura et al., 2012, 2013; Shiraishi et al., 2018).

This work presents a fossil system of perched and fluvial travertines passing distally to fluvial tufas within a volcanic ravine. The absence of tectonic and volcanic activity affecting the area during deposition times should indicate climate and hydrogeology as determining factors. Facies characteristics and their relationships, together with geochemical data were analysed to study relations between microbial and crystal growth rates in our case. Facies associations were also analysed to

<sup>\*</sup> Corresponding author.

E-mail address: [arberiguete@ucm.es](mailto:arberiguete@ucm.es) (Á. Rodríguez-Berriguete).

study sedimentary conditions leading to either microbial-related or inorganic-dominated  $\text{CaCO}_3$  precipitation, in order to understand: (i) the formation of these carbonates in that setting; (ii) relationships between facies, as well as (iii) the parameters controlling evolution from proximal travertines to distal tufas.

## 2. Setting

The deposits studied are located in the Azuaje Ravine, in the North of Gran Canaria Island (Canary Islands, Spain), along a stretch of about 3 km (Fig. 1). This ravine trends approximately SSW-NNE, incised about 300 m in volcanic rocks, mostly Pliocene breccias and lavas (Roque Nublo Fm) and Pliocene-Pleistocene lavas (Post-Roque Nublo Fm) which overlie Miocene phonolites unconformably, that outcrop in scattered areas (Balcells et al., 1992; Pérez-Torrado et al., 1995; Carracedo et al., 2008). The ravine parallels a passive normal fault with an eastern hanging wall block affecting Miocene to Pleistocene

rocks (Rodríguez Berriguete, 2017). A Holocene intracanyon lava (Doramas lava) at the bottom of the ravine (Rodríguez-Gonzalez et al., 2009) is generally older than the carbonate deposits, shows an erosive surface as well as clastic deposits between lava and overlying carbonate deposits (Rodríguez Berriguete, 2017).

Several isolated carbonate deposits appear along a stretch of the Azuaje Ravine. Travertines appear perched on ravine walls, and lower, in fluvial position (Rodríguez-Berriguete et al., 2012), whereas tufa deposits appear exclusively at the bottom of the ravine and downstream from travertine deposits (Fig. 1). Fluvial activity has eroded carbonate deposits and intracanyon lava (Rodríguez Berriguete, 2017).

Springs in the area are dry and there is no current carbonate deposition. Groundwaters of the area are bicarbonate-Na-Mg-Ca rich, with pH below 7 in general, and Mg/Ca ratios above 1, in some cases exceeding 10. Groundwater temperatures generally are about 25 °C at most, occasionally reaching >30 °C, and  $\text{CO}_2$  contents are higher than 150 mg/l (SPA-15, 1975; Hernández-Quesada, 2016).

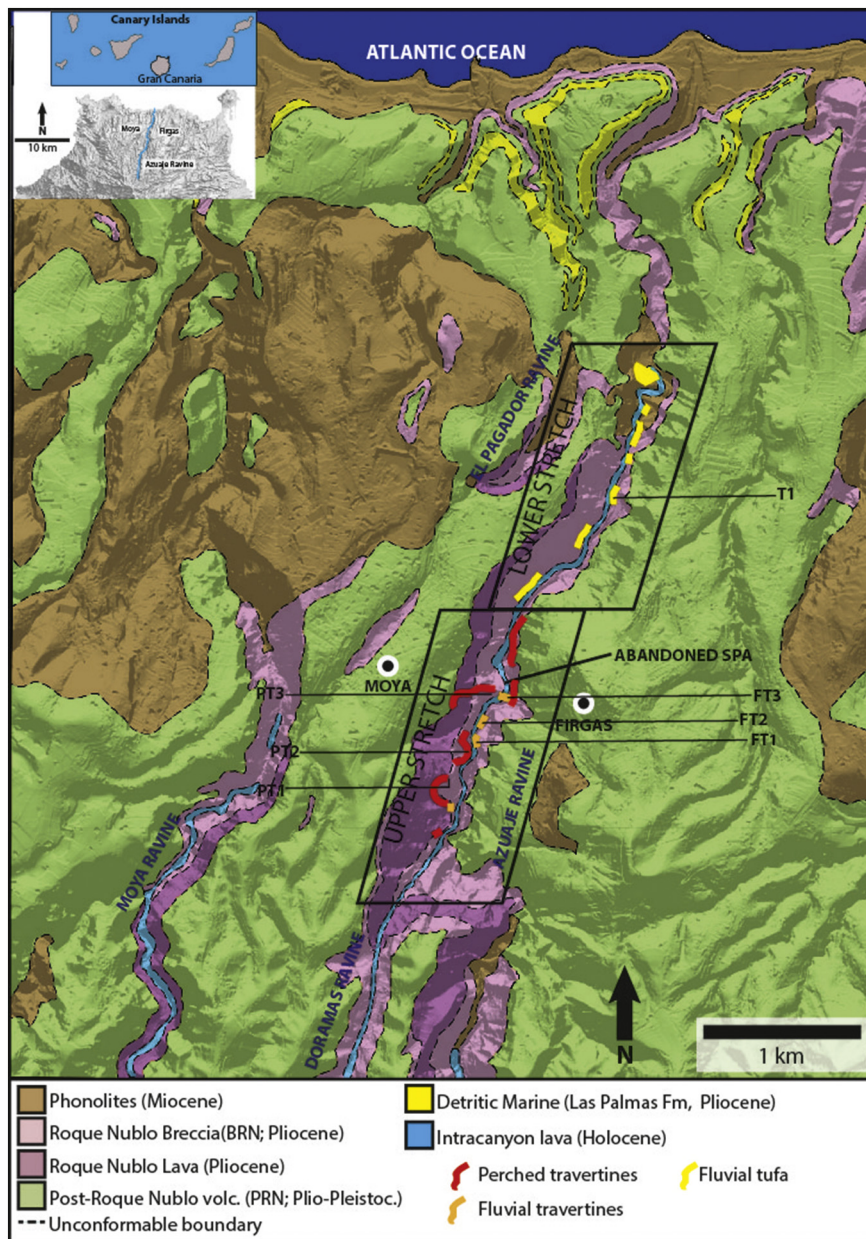


Fig. 1. Location of island of Gran Canaria (Canary Islands), Azuaje Ravine (mdt + 5, PNOA yielded by © National Geographic Institute) and Geological map of region comprising the study area and distribution of travertine and tufa deposits (modified from: Balcells et al., 1992 (MAGNA 1101 - III) and Rodríguez-Gonzalez et al., 2009). PT: perched travertine; FT: fluvial travertine; T: tufa.

Climate in Gran Canaria, controlled mainly by trade winds and the great relief of the centre of the island, brings more humidity in the northern flank than in the southern one. Mean annual temperatures are about 20 °C. Torrential rainfalls exceeding 800 mm/year occur mainly in winter, mostly at the high altitudes of the northern flank of the island (Marzol Jaén and Máyer Suárez, 2012; Mestre and Felipe, 2012).

### 3. Methodology

117 thin sections were studied by using an Olympus BX51 optical microscope with an Olympus U-TVO.5XC-3 camera; thin sections (8) and freshly broken fragments (15) were studied by using scanning electron microscopy coupled to EDS and CL detectors (respectively, a JEOL JSM 6400 at CNME-UCM, and a FEI INSPECT with a GATAN Mono CL3 for cathodoluminescence (CL) analyses, at MNCN-CSIC) both working at 20 kV. X-ray diffraction (XRD) analyses (Phillips PW-1710 X-ray diffraction (XRD) system) were performed on 192 samples at 40 kV and 30 mA under  $\text{CuK}\alpha$  radiation at IGEO (CSIC); identification and percentages of mineral phases were estimated by using EVA software (Bruker). A wavelength dispersive electron probe microanalyser (WDS-EPMA), model JEOL JXA 8900 M (JEOL Limited) at the ICTS-CNME, Complutense University of Madrid, Spain, was used to determine proportions and distribution of the main elements contained in 4 carbon-coated, thin sections. Stable isotopes from 83 samples were analysed at Scientific-technic Services of Barcelona University and corrected using the NBS-19 standard, providing reproducibilities for C and O respectively of 0.01 and 0.05.  $^{87}\text{Sr}/^{86}\text{Sr}$  analyses of 9 samples were carried out in the Centre for Research Assistance in Geochronology and Geochemistry of the Complutense University (Madrid, Spain), providing  $2\sigma$  of  $1.4 \times 10^{-5}$ . Datings by U/Th method were performed at Jaume Almera Earth Sciences Institute-CSIC (Barcelona, Spain) by using an Alpha spectrometer ORTEC OCTETE PLUS (8 Detectors BR-024-450-100) for  $^{234}\text{U}/^{230}\text{Th}$ ,

on 8 selected samples with very low siliciclastic contents, from bases and/or tops (depending on accessibility for sampling) of all the studied deposits. Weight of subsamples was 20 g.

### 4. Results

#### 4.1. Distribution and characteristics of the deposits

Travertines and tufas studied in the present work have been differentiated based on textural features and observed facies. Travertines display a more crystalline, less porous texture (Fig. 2A–C), and typical facies are shrubs, dendrites, rafts, ooids, and dense laminated stromatolites. Tufas display a micritic aspect, are much more porous (Fig. 2D), contain abundant vegetal-related facies, and typical facies are coated stems, oncoids, intraclasts (mainly those of broken coated stems), phytoclasts and both porous and dense laminated stromatolites.

##### 4.1.1. Travertine deposits

Along the upper stretch of the study area the altitude of the travertine deposits varies higher than 300–200 m asl of the bottom of the ravine (Fig. 1A). They can be found perched on the ravine sides, or close to the bottom of the ravine in fluvial position.

**4.1.1.1. Perched travertines (PT).** Found along the upper stretch of the study area mostly on the western side of the ravine, except in the lower part of this upper stretch, where they also appear on the eastern side (Fig. 1). Perched deposits ranging from 4 m to several tens of metres in height, and several tens of metres in width are located between 5 and 150 m above the current bottom of the ravine. Three perched deposits on slopes varying from horizontal to almost vertical were studied (Fig. 2A, B).

**4.1.1.2. Fluvial travertines (FT).** 1.5 to 4.0 m in thickness and up to 10 m in length, mostly on the eastern side, in contact with the upper surface of

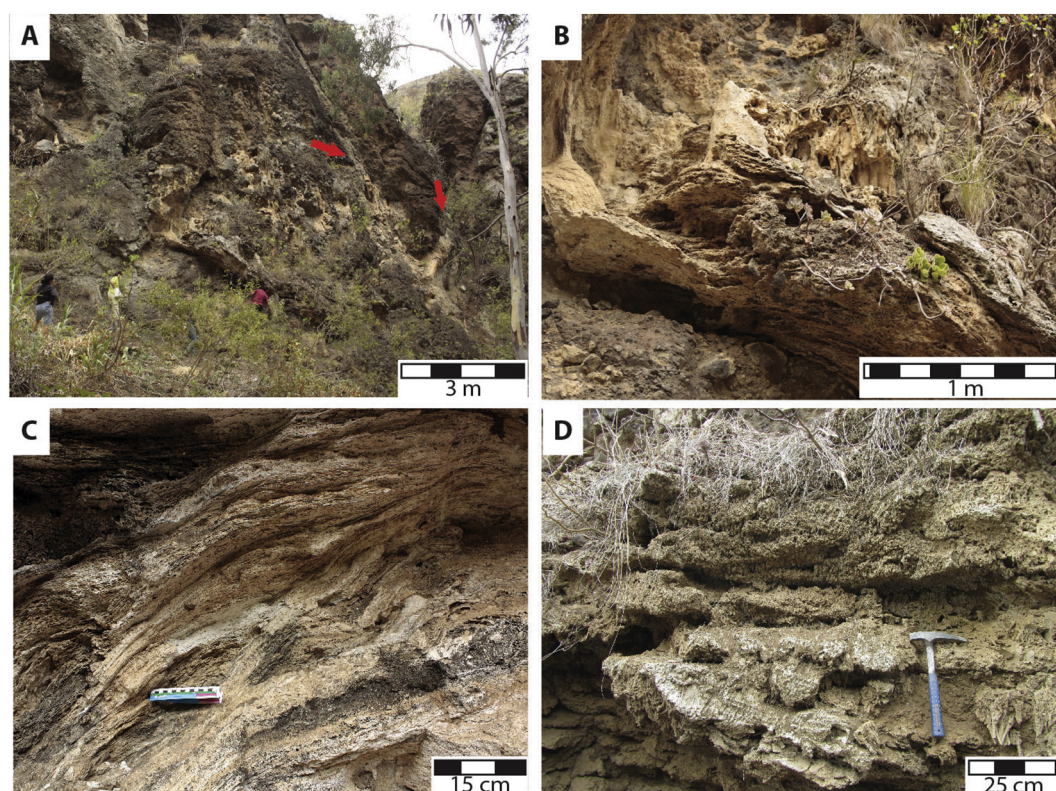


**Fig. 2.** A. View of PT3 outcrop, where fractures and related carbonate deposits (arrows) are seen. B. Mound of carbonate developed on step of hillside. In background hanging coated stems are observed. C. Clinoforms from a fluvial deposit (FT3). D. View of distal fluvial tufa (T1).

the intracanyon lava in all cases (Fig. 1), generally 5–10 m above the bottom of the ravine with their major dimension parallel to it, although in some cases such variation in elevation may be partly the consequence of collapse of lava tubes. Deposits formed on steps of the bottom of the ravine have vertically aligned arrangements and mound-like morphologies (Fig. 2C), whereas those formed on relatively lower slopes display wedge-like morphologies. Where visible, bases of deposits are in erosive discontinuity with the top of lava or there is a detrital deposit between both lava and travertine. The magnitude of erosive discontinuities is also observable within the fluvial travertines at several scales.

#### 4.1.2. Tufa deposits (T)

These deposits, in fluvial position, first appear a few metres downstream from the last travertine along the lower stretch of the area studied (bottom of the ravine altitude 200–90 m asl) (Fig. 1), with bases laying on the intracanyon lava, 1–2 m above of the bottom of the ravine. Lava-tufa boundary is in some cases erosive, in others there may be an intercalation of a clastic deposit of well-rounded boulder to sand-sized volcanic rock fragments cemented by carbonates. Tufa deposits were incised and exposed after the end of sedimentation due to fluvial erosion, as in the case of fluvial travertines upstream.

These tufa deposits, several tens of metres long, reach maximum thicknesses of 3.0–4.5 m (Fig. 2D). They display a wedge-like morphology with decreasing thickness downstream, related to both short steps and along gently sloping stretches of the ravine.

#### 4.2. Facies and microfacies

Travertine and tufa facies have been classified into two broad categories: (i) facies formed in situ, on a fixed substrate, with initially bound components (boundstones; crystalline crusts); (ii) facies formed by initially loose particles, including wackestones-grainstones and rudstones (ooids, oncoids, rafts, phytoclasts, coated bubbles, fragments of coated stems).

##### 4.2.1. Facies formed in situ, on a fixed substrate, with initially bound components

**4.2.1.1. Laminated or stromatolitic boundstones.** May consist of (i) dense or (ii) porous laminae. The dense laminae (i) are composed of planar to wavy or crenulated lamination, displaying variable thicknesses (Fig. 3A, B), sometimes developing dome or columnar morphologies. They may be micritic or fibrous laminae, composed of densely packed fibres arranged perpendicular to the substrate. Porous laminae (ii) show thicker laminae or bands than the dense ones. Porous laminae can be micritic, microsparitic, and more exceptionally sparitic (Fig. 3B).

Micritic filaments normally arranged perpendicularly to the substrate are commonly present. Pores are of hundreds of micrometres to almost 1 mm in size, with irregular morphologies and commonly showing their largest dimension parallel to the filaments. Dense and porous laminae, with more irregular morphologies, are notably thicker in distal tufas than in travertines.

**4.2.1.2. Dendrites and shrubs.** They consist of polycrystals with arborescent morphologies, generally growing perpendicularly or obliquely to the substrate. Both occur in a wide diversity of shapes, with different development of branching, as well as with variable density between their branches, thereby leaving variable pore sizes of several hundred micrometres, up to 5–6 mm long (Fig. 4). Shrubs are formed by fibrous-acicular aragonite crystals (Fig. 4A, B), whereas dendrites consist of several branches formed by stacked platy rhombic calcite crystals (Fig. 4C, D). Dendrites/shrubs can form centimetre to decimetre size patches or small mounds, or they can form bands or layers parallel to the substrate in both perched and fluvial travertines.

**4.2.1.3. Boundstones of bryophytes.** This facies consists of crusts developed around moldic pores from decomposed parts of bryophytes. Crusts are finely laminated showing an alternating banded (Fig. 5A), micritic, exceptionally fibrous texture. Boundstones of bryophytes were found in perched travertines and in some cases in fluvial tufas, but not in fluvial travertines.

**4.2.1.4. Boundstones of coated stems.** Coated stems are cylindrical structures consisting of a hollow core surrounded by one or several concentric coatings of calcite (Fig. 5B). The central void is a moldic porosity left by decomposition of different parts of plant stems or branches. Coating textures, like those described for the stromatolitic (and also dendritic, in perched travertines) boundstones, vary along the ravine. Coated stems can be arranged (i) in palisades of vertical stems forming patches, or (ii) in bundles of hanging stems pointing in downflow direction. They appear in fluvial tufas and in some perched travertines.

**4.2.1.5. Crystalline facies.** Crystalline facies are crusts of acicular (widths of 10  $\mu\text{m}$  or less) to prismatic (widths of several tens of  $\mu\text{m}$ ) crystals of several hundred micrometres to several millimetres in length, growing normal to the substrate (Fig. 6A, B). Crystalline crusts commonly show a barely marked banding, in some cases corresponding to interruptions in crystal growth (Fig. 6A). These crusts appear in: (i) filled syn-depositional fractures in a few perched travertines, affecting both the substrate and the carbonate deposit itself (Figs. 2A, 6A); and (ii) in bedding planes related to steep slopes of perched and fluvial travertines.

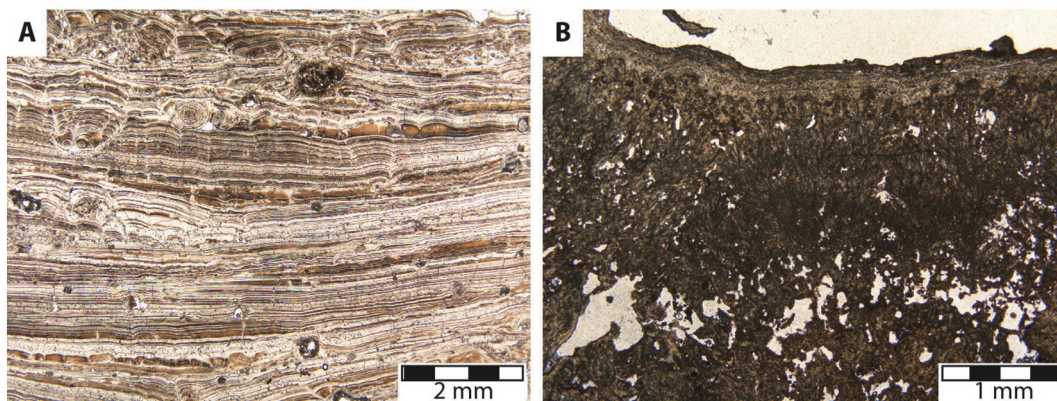


**Fig. 3.** Optical microscope images of: A. Dense stromatolitic lamination with light-dark alternation (perched travertines). B. Thick porous micritic lamina passing to thin dense lamina with wavy lamination on top (fluvial tufas).

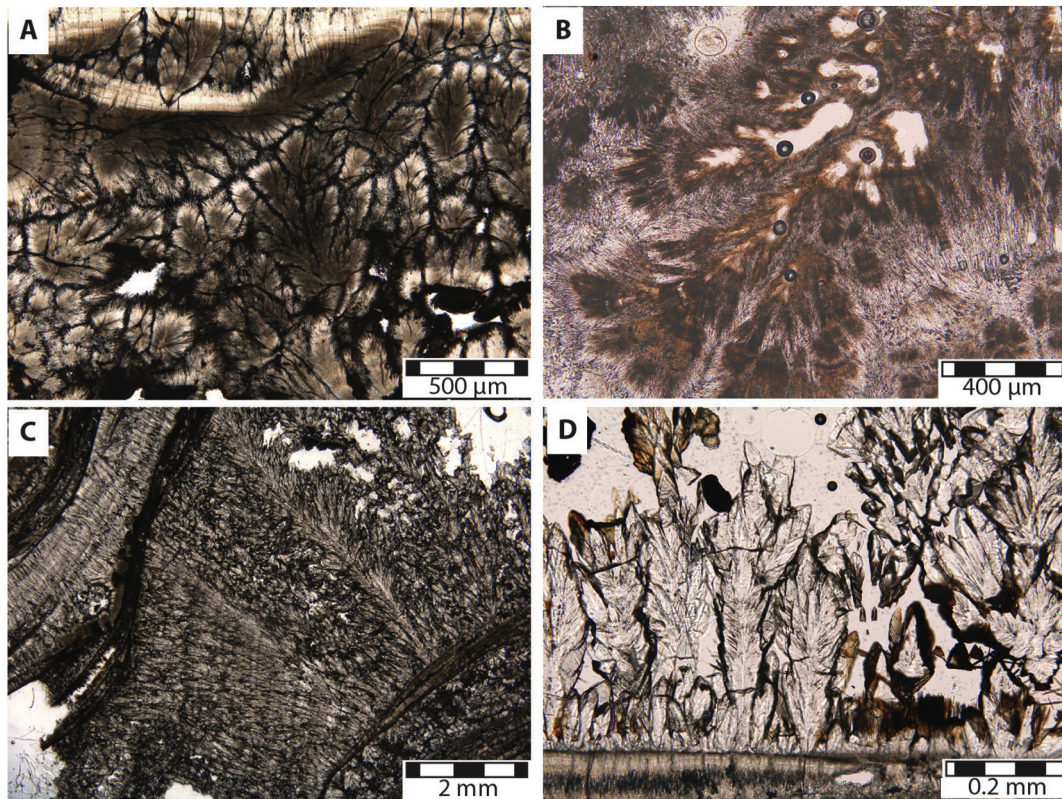


**Fig. 4.** Optical microscope images of: A. Fibrous shrubs from fluvial travertine. B. Fibrous shrubs where recrystallization and/or cementation is observed in matrix in addition to dissolution. C. Inclined layers of calcitic dendrites with significant vertical development (fluvial deposits). D. Image of calcitic dendrites (perched deposits), where detail of dendrite branch can be seen in upper left part, showing offset stacking of flat rhombs.

#### 4.2.2. Facies formed by initially loose particles

**4.2.2.1. Rudstone to wackestone rafts.** Rafts are platelets a few micrometres thick and up to several centimetres wide (Fig. 7A, B) surrounded by acicular crystals growing perpendicular or fan-shaped, with crystals longer in the lower than in the upper face of platelets (Fig. 7A).

Rafts can accumulate approximately parallel to deposit bedding, leaving horizontally elongated milli-centimetre, shelter porosity, which is partially to fully cemented by acicular crystals. Rudstone rafts, in some cases packstone-grainstone, rarely wackestone and floatstone rafts are common in these perched and fluvial travertines.

**4.2.2.2. Packstone-Grainstone ooids.** These ooids, of spherical to oval morphologies (Fig. 8A, B), have diameters varying 100 µm–3 mm,

in general. Nuclei are frequently travertine intraclasts, more rarely phytoclasts. Occasionally nuclei are indistinguishable from the coatings or can even be absent. Coatings generally consist of a concentric alternation of smooth light and dark laminae of 1–5 µm thickness. Laminae forming the dark-light couples can be (i) both micritic (Fig. 8A), or (ii) light fibrous and dark micritic, or (iii) both superimposed on, or cut by, radially arranged fibrous crystals (Fig. 8C) with lengths equal to the thickness of the cortex. Ooids are restricted to travertines.

**4.2.2.3. Wackestone-packstone-grainstone coated bubbles.** Coated bubbles are spherical particles of 10 µm–2 mm in diameter, composed of a hollow core and a very thin micritic coating surrounding the core (Fig. 8D). Micritic coatings can also be surrounded by fibrous, acicular, prismatic and dendritic crystals (Fig. 8E). The central void can be partially or totally cemented by fibrous to acicular crystals. Coated

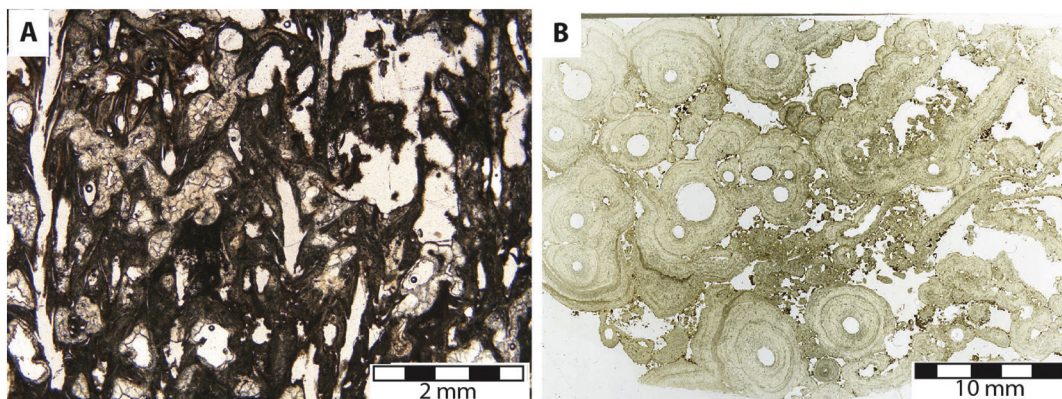


**Fig. 5.** A. Boundstone of bryophytes showing vertical moldic porosity partially cemented by sparite. B. Scanned thin section showing transversal section of boundstone of coated stems from fluvial deposits.

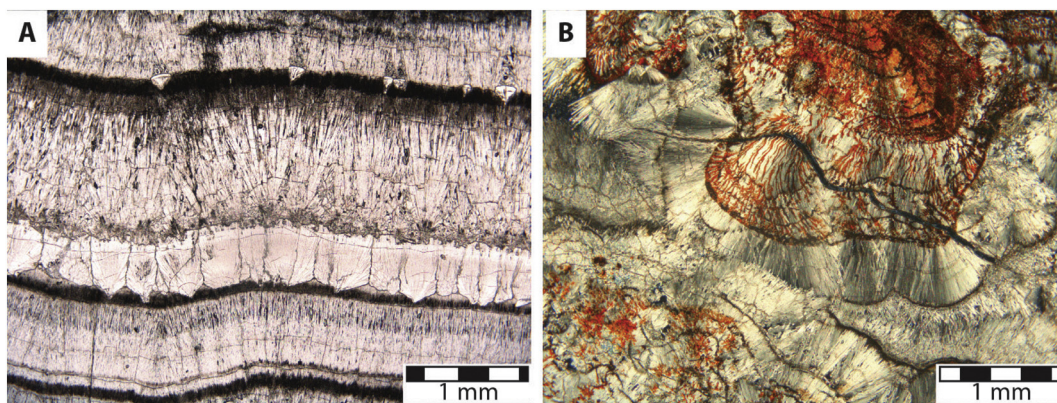


**Fig. 6.** Microscope images of primary crystalline facies: A. Crystalline crust of fibrous crystals in fracture of volcanic substrate (perched travertines) with micritization in apices and cementation-recrystallization in some bands. B. Fibrous-acicular crystals with concentric disposition, containing Fe oxides or oxi-hydroxides with flame texture of speleothem (perched travertines).

bubble accumulations occasionally show grading and are either cemented by fibrous crystals or included within a micritic matrix. Gas escape structures were not observed. This facies appears in perched and fluvial travertines, related to pool and barrier-waterfall subenvironments in short vertical steps.

**4.2.2.4. Wackestone to rudstone phytoclasts.** Consist of micrite with abundant moldic porosity of plant remains (Fig. 8F), partially preserved in some cases. Neither the preserved remains nor the moulds left by decomposition of plant material have coatings. Phytoclastic accumulations commonly occur in perched travertines, also in distal tufas, being less frequent in fluvial travertines.

**4.2.2.5. Wackestone to rudstone oncoids.** Travertine oncoids have spherical to oval morphologies (Fig. 9) and diameters from 100  $\mu\text{m}$  to >1 cm. Nuclei of these travertine oncoids are intraclasts and phytoclasts, on occasions indistinguishable from the cortex, or entirely absent. Coatings consist of alternating wavy, light and dark laminae each one of 1–2  $\mu\text{m}$  thickness or smaller. Both of them can be (i) micritic (Fig. 9A, B), or (ii) the light laminae can be fibrous and the dark ones micritic. The cortex can be composed of dendrites radiating from the centre of the oncoid (Fig. 9B–D). Oncoids are included in micritic matrices with a high content of detrital material (extraclasts), or they may be cemented, appearing in pool-barrier sub-environments.

Tufa oncoids present varied morphologies and sizes ranging from <1 mm to up to 20 cm, depending on the type of nuclei, commonly phytoclasts or intraclasts (Fig. 9E). Coatings are formed by just 2–3 laminae, generally thicker than in travertine oncoids, showing micritic

texture, although a very fine fibrous texture was also observed. Tufa oncoids accumulated forming mounds and tabular layers in cascade sub-environments.

A special case is that of decimetre size tufa oncoids with a palm leaf raquis nucleus. Coatings in this case are alternating thick porous micritic laminae and thinner dense micritic to fibrous laminae (Fig. 9F), analogous to stromatolite boundstones of Azuaje tufas.

**4.2.2.6. Grainstone, rudstone of coated stems (or other plant parts).** This facies consists of accumulated fragments of coated, broken plant parts. Fragments of coated plant parts can be mixed indistinguishably with oncoids.

#### 4.3. Relations between facies

Travertines and tufas show vertical and lateral facies changes on different scales, as well as alternations between the two facies giving rise to vertical stacking of several repeated beds. Relationships between travertines facies and tufa facies are separately described and interpreted in the following.

##### 4.3.1. Travertine facies associations, variations and alternations

**A. Rudstones of oncoids and stromatolitic boundstones:** Oncoid accumulations are commonly overlaid by dense, thin stromatolite boundstones, forming either mounds or tabular layers (Fig. 10A). Oncoids and stromatolites commonly alternate giving rise to vertical stacking of beds of these two facies.

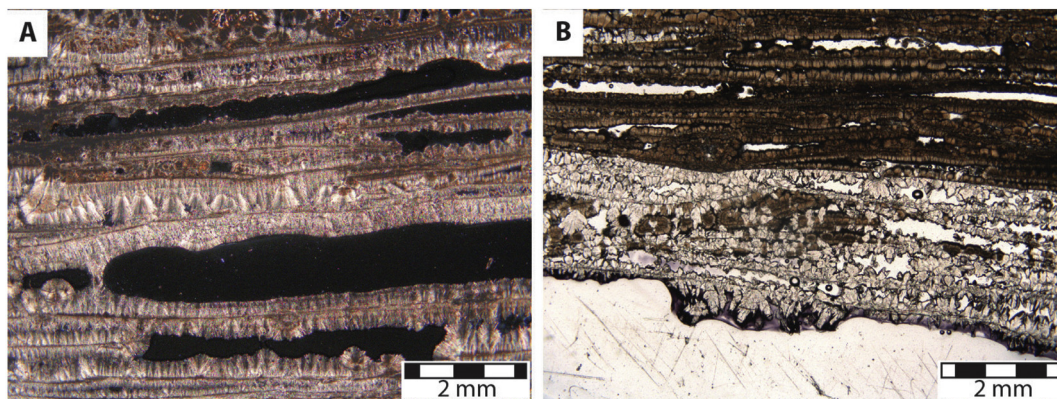


**Fig. 7.** Microscope images of rafts: A. Rudstone of fibrous crystal rafts with shelter-type porosity (fluvial travertines). B. Rudstone of rafts of rhombic crystal (base, light colour) and fibrous crystals (top, brown) (perched travertines).

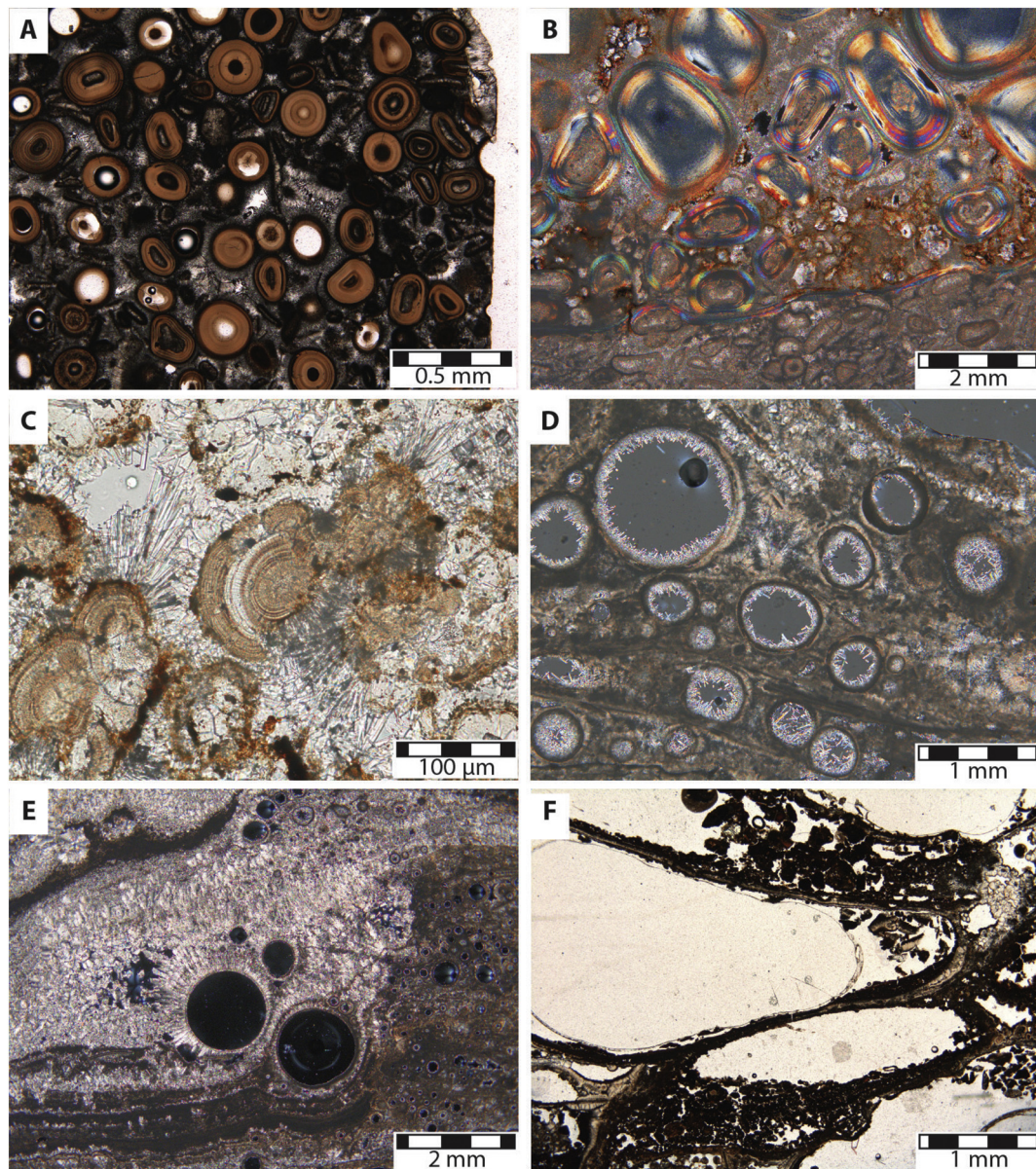


**Fig. 8.** Microscope images: A. Grainstone of concentric ooids cemented by acicular crystals (perched travertines). B. Packstone to rudstone of ooids with increasing-size trend in silt-clayey matrix partially recrystallized with microsparite (fluvial deposits). C. Ooids of fibrous-radiated crystals cemented by acicular crystals and with features of recrystallization (perched deposits). D. Bubbles alternating with micrite bands (fluvial deposits). E. Small bubbles in laminated micritic matrix (lower part of the image) and larger bubbles surrounded by prismatic and dendritic crystals around in matrix with recrystallization features (fluvial deposits). F. Intraclastic grainstone with abundant morphological porosity of phytoclasts (originally phytoclastic wackestone-packstone) (perched deposits).

- B. Rudstones of oncoids and dendrite boundstones: Similar to the previously described oncoid-stromatolite associations, but with dendrites instead stromatolites overlaying oncoids. Alternations are much less common than in the case of oncoid-stromatolite associations.
- C. Rudstones of rafts and dendritic boundstones: Raft accumulations of several millimetres thickness can overlie bands of dendritic boundstones or can vertically and laterally become these dendrites (Fig. 10B). These two facies in some cases appear alternately.
- D. Boundstones of dendrites and boundstones of laminar stromatolites: Most commonly they alternate (Fig. 10C), although in some cases lacking a defined pattern of repetition or alternation.

#### 4.3.2. Tufa facies associations, variations and alternations

- A. Dense-porous stromatolitic boundstones: dense, thin laminae are the most commonly observed stromatolitic lamination in these deposits. Stromatolites are commonly related to other facies as

described below. Thicker porous micritic laminae containing filaments are less common. However, sometimes both porous and dense laminae appear as alternations (Fig. 11A).

- B. Rudstone of oncoids-stromatolitic boundstones: oncoids can accumulate forming mounds or fluvial bars, or can form millimetre to centimetre thick beds, in both cases subsequently encrusted by (mostly dense) stromatolite laminae of a few mm thickness. The centimetre thick beds usually appear as alternations of both facies (Fig. 11B).
- C. Rudstones of phytoclasts and/or intraclasts-stromatolitic boundstones: phytoclasts usually appear forming beds of several centimetre thickness encrusted on their tops by a very thin stromatolitic laminae, sometimes producing alternations of both facies (Fig. 11C).
- D. Boundstones of coated stems bounded by discontinuities: patches and horizontal beds of vertically arranged calcified plants appear repeatedly stacked, or in some cases alternate with thin stromatolitic laminae (Fig. 11C).

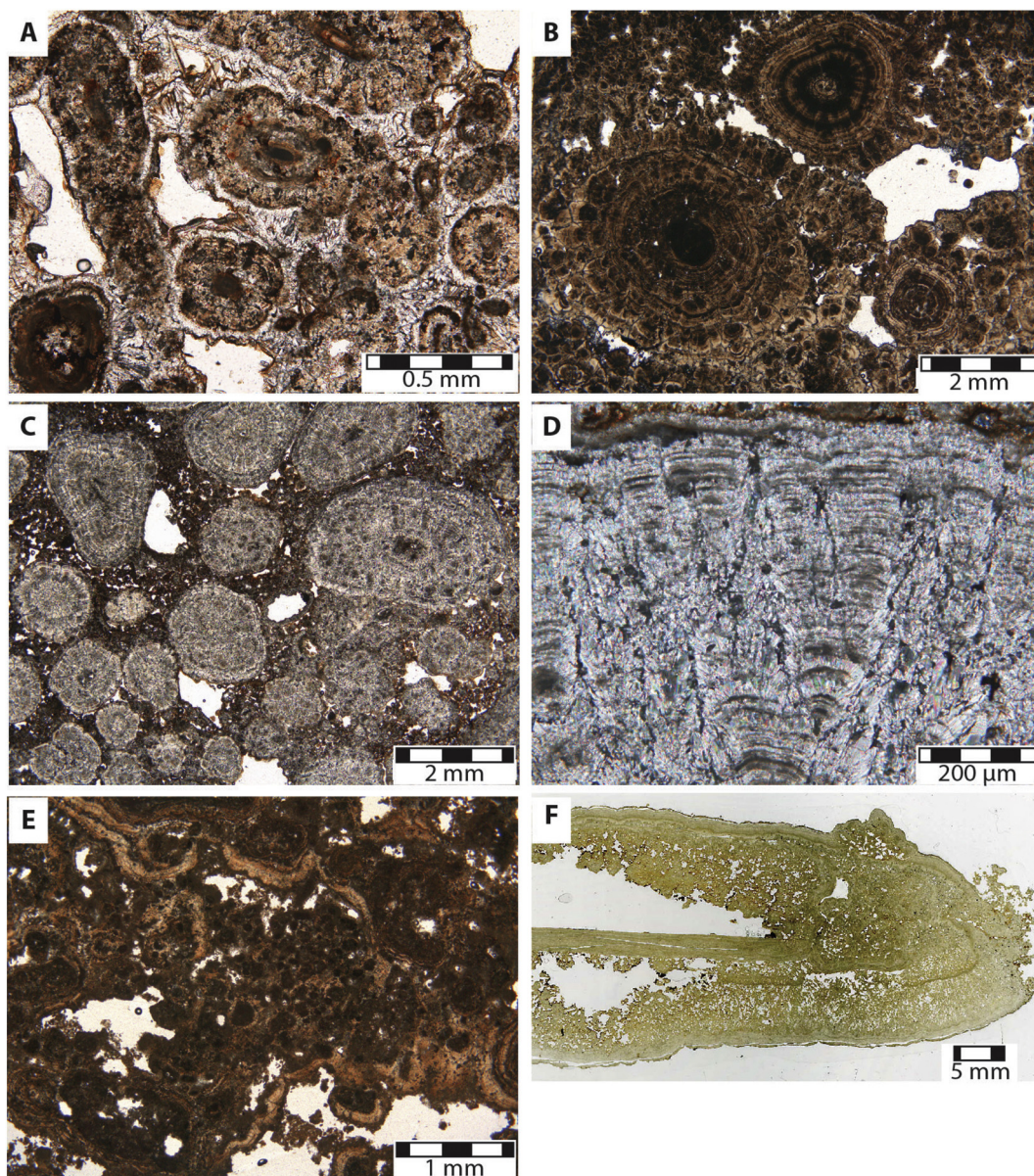


**Fig. 9.** Optical microscope images of oncoids: A. Grainstone of oncoids with spherical and elliptical morphologies, cemented by sparite (perched travertines). B. Grainstone-rudstone of oncoids with micritic mamelonated lamination (fluvial travertines). C. Packstone-rudstone of oncoids in micritic-clayey matrix (perched travertines). D. Detail of oncoid from C, with alternating fibrous, partially recrystallized lamination that forms columnar developments in the oncoid cortex. E. Grainstone of oncoids from tufa deposits with thicker and irregular laminae than in travertines upstream. F. Scanned thin section with part of an oncoid formed around the raquis of palm leaf subsequently dissolved leaving moldic porosity.

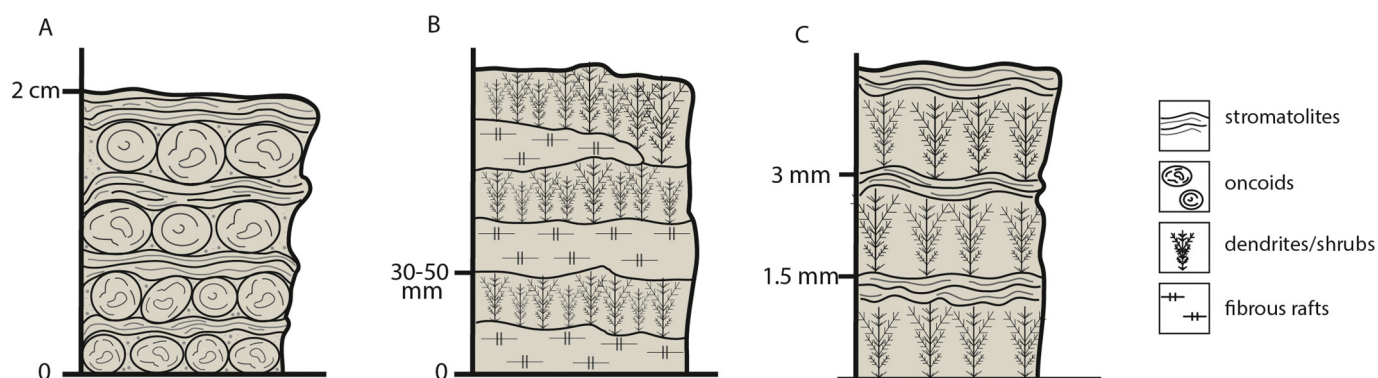


**Fig. 10.** Sketch of different travertine facies relationships and alternations from Azuaje: A. Stromatolites-oncoids; B. Rafts and dendrites/shrubs; C. Dendrites/shrubs and stromatolites.

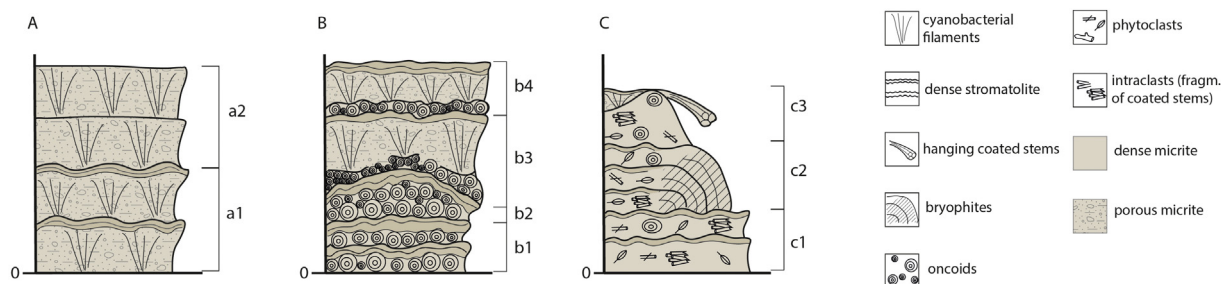


**Fig. 11.** Sketch of different tufa facies relationships and alternations from Azuaje: A. Dense and porous stromatolite boundstones; B. Oncoids and dense/porous stromatolite boundstones; C. Phytoclasts and stromatolite, bryophyte and hanging-coated stem boundstones.

#### 4.4. Mineralogical composition

Perched and fluvial travertines have aragonitic, calcitic and mixed aragonitic-calcitic compositions. Aragonite is dominant in both perched and fluvial travertines with no clear trend in aragonite-calcite proportions. However, calcite proportions are also important as can be seen in common calcitic travertine facies. Distal fluvial tufas are exclusively calcitic. Manganese and iron oxides and oxi-hydroxides are present in trace amounts not only mainly in perched but also in fluvial travertines. Detrital input of volcanic minerals such as feldspars, piroxenes or foids is observed.

#### 4.5. Element geochemistry

Aragonite contents 99 mol%  $\text{CaCO}_3$  or higher (Table 1). That is, <1 mol% corresponds to carbonates of other metals, almost all of them below detection limits of EDS.  $\text{SrCO}_3$  is present in all analyses performed by EMPA, with contents generally above 0.5%mol.  $\text{BaCO}_3$  and  $\text{Na}_2\text{CO}_3$  can be present in very small amounts or can be absent (or below detection limits of EMPA).  $\text{MnCO}_3$  can also appear in very small amounts, or apparently can be absent according to EMPA, although  $\text{Mn}^{2+}$ -activated cathode-luminescence was observed in all aragonites analysed, with a decrease in  $\text{MnCO}_3$  content from perched to fluvial travertines (Fig. 12).

Calcite, of 94–96 mol%  $\text{CaCO}_3$  (exceptionally 90 mol%) (Table 1), was composed of 4–6 mol% of carbonates of other metals.  $\text{MgCO}_3$  is present in all calcites analysed from travertines and tufas, with contents of 1–4 mol% (exceptionally exceeding 5 mol%).  $\text{SrCO}_3$  is also present generally below 0.5 mol% in all calcites analysed.  $\text{MnCO}_3$  is present in travertine calcites in amounts detectable by EDS, but below that limit in tufa calcites. Contents are generally below 2 mol% in perched and fluvial travertines as has been measured by electron microprobe (EMPA), but with a decreasing trend in  $\text{Mn}^{2+}$  content from perched to fluvial travertines, and decreasing even more to fluvial tufas. The evidences for such decrease in divalent manganese are (i)  $\text{Mn}^{2+}$  is detected in calcites from travertines by EDS analyses but it is not detected in tufa calcite; (ii) CL peaks decrease in intensity from travertines to tufas (Fig. 12), demonstrating that  $\text{Mn}^{2+}$  is present in tufa calcite but in lower amounts than in travertine calcite, below the detection limit of EDS.  $\text{FeCO}_3$  is also present in small amounts, below 2 mol% and with a rapid downstream decrease from perched to fluvial travertines. Calcite has lower  $\text{Fe}^{2+}$  than  $\text{Mn}^{2+}$  contents in general, and although commonly present,  $\text{Na}_2\text{CO}_3$  contents are below 0.5 mol%.

**Table 1**

Summary of geochemical compositions of aragonite and calcite from Azuaje carbonates based on EDS, CL and EMPA data.

	$\text{CaCO}_3$	$\text{MgCO}_3$	$\text{MnCO}_3$	$\text{FeCO}_3$	$\text{SrCO}_3$	$\text{Na}_2\text{CO}_3$	$\text{BaCO}_3$
Aragonite	>99	–	– (CL)	–	0.5–0.3	0.3–0.6	<0.1
Calcite	94–96	1–4	<2	<2	<0.5–0.0	<0.5–0.0	<0.1

#### 4.6. Isotope geochemistry

##### 4.6.1. $\delta^{13}\text{C}$ – $\delta^{18}\text{O}$

Stable isotope values of the Azuaje travertines and tufas range from –2.08 to –11.55‰ V-PDB for  $\delta^{18}\text{O}$ , and from +3.60 to +14.32‰ V-PDB for  $\delta^{13}\text{C}$  (Fig. 13; Table 2). Perched travertines range from –2.15 to –11.55‰ V-PDB in  $\delta^{18}\text{O}$  and from +14.32 to +3.78‰ V-PDB in  $\delta^{13}\text{C}$ . Fluvial travertines range from –2.08 to –10.41‰ V-PDB in  $\delta^{18}\text{O}$  and from +10.78 to +4.36‰ V-PDB in  $\delta^{13}\text{C}$ . Finally, fluvial tufas range from –4.44 to –5.33‰ V-PDB in  $\delta^{18}\text{O}$  and from +6.11 to 3.60‰ V-PDB in  $\delta^{13}\text{C}$ .

However, the wide range in  $\delta^{18}\text{O}$  values is the consequence of the lower  $\delta^{18}\text{O}$  values of just two deposits with special features within the ravine. If these outliers are excluded, then  $\delta^{18}\text{O}$  values range from –2 to –6‰ V-PDB for the rest of travertines and tufas. In consequence,  $\delta^{13}\text{C}$  values range from +3.60 to +14.32‰ V-PDB, with tufa  $\delta^{13}\text{C}$  below +6‰ V-PDB, therefore generally lower than  $\delta^{13}\text{C}$  from travertines.

Compared to other deposits, Azuaje travertines show a larger range of variation in both stable isotopes (Fig. 13), whereas Azuaje tufas fall in a narrow range similar to those of other tufas from N Gran Canaria (Camuera et al., 2014; Rodríguez-Berriguete et al., 2018).

Travertines and tufas are clearly differentiated by their  $\delta^{13}\text{C}$  signal, clearly lower (although positive) for tufas than for travertines.

##### 4.6.2. $^{87}\text{Sr}/^{86}\text{Sr}$

Travertines from Azuaje Ravine display  $^{87}\text{Sr}/^{86}\text{Sr}$  values from 0.703765 to 0.703361 (Table 3), with no clear differences between perched and fluvial travertines and tufas. These values are close to those reported for volcanic rocks of the Canary Islands, including Gran Canaria (Cousens et al., 1990; Ovchinnikova et al., 1995; Thirlwall et al., 1997; Abratis et al., 2002; Hansteen and Troll, 2003), and more precisely, are close to the values of Miocene rocks, with a  $^{87}\text{Sr}/^{86}\text{Sr}$  higher than in those of Plio-Pleistocene volcanic rocks (Abratis et al., 2002; Aulinas et al., 2010). This is also in agreement with  $^{87}\text{Sr}/^{86}\text{Sr}$  of groundwaters of the area, which have been interpreted as due to a predominance of groundwaters from the deep Miocene aquifer (Hernández-Quesada, 2016).

Spatial distributions of  $^{87}\text{Sr}/^{86}\text{Sr}$  values show no  $^{87}\text{Sr}/^{86}\text{Sr}$  values differences between all the perched travertines (Table 3; Fig. 1). Values for fluvial travertines and tufas are also very similar, with one exception (FT2), showing that the water supply to the fluvial system was dominantly the same than record the perched deposits studied in this work.

#### 4.7. Age of the travertines and tufas

U/Th datings generally range from 2892  $^{+139}_{-139}$  to 3696  $^{+392}_{-390}$  y BP (Table 4). Perched deposits show older ages and wider ranges than fluvial deposits. Minimum ages of perched deposits range at least from 3.0 to 3.7 ky BP whereas fluvial deposits ages

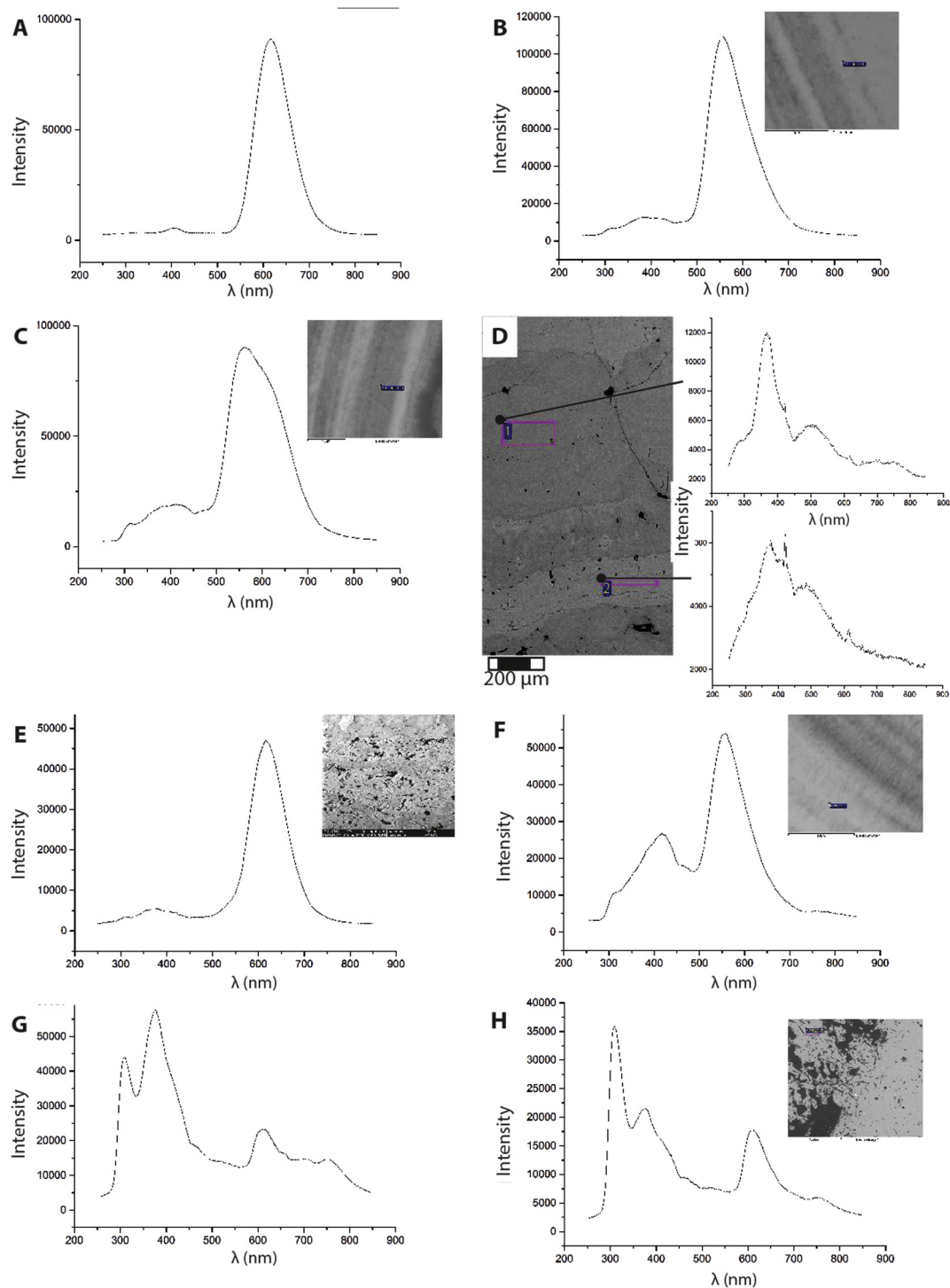


**Fig. 12.** Catodoluminescence (CL) spectra: A.  $\text{Mn}^{2+}$ -activated CL in calcite of oncoids from a perched travertine. B.  $\text{Mn}^{2+}$ -activated CL in aragonite of ooids from a perched travertine. C.  $\text{Mn}^{2+}$ -activated CL in an aragonitic sample of ooids with a variable calcite content, from a perched travertine. D. CL spectra obtained on (1) a darker zone of calcitic composition, and (2) a lighter zone where there is no activation by manganese and the intrinsic luminescence pattern of the carbonate (fluvial travertine) is observed. E.  $\text{Mn}^{2+}$ -activated CL in calcite of rafts and crystalline crusts from a fluvial travertine (the shoulder suggests a certain content in aragonite). F.  $\text{Mn}^{2+}$ -activated CL in aragonite, from an oncoid of a fluvial travertine, where the intrinsic luminescence pattern of the carbonate is also observed. G.  $\text{Mn}^{2+}$ -activated CL spectrum, together with intrinsic CL of calcite of a coated stem of a distal deposit. H. CL spectrum where the intrinsic carbonate luminescence dominates, although a low intensity peak due to  $\text{Mn}^{2+}$ -activated luminescence is also observed in a stromatolytic sample from a distal tufa deposit.

range from 2.9 to 3.3 ky BP. The older ages of perched travertines were obtained from samples near the base of the deposits. Whereas fluvial travertines have maximum ages of about 3.3 ky BP near the base of the deposits.

Distal tufa deposits were not successfully dated. Just one dating of about 11 ky BP, was obtained from a sample found within a channel

incised in intra-canyon lava. However, this age was rejected, in part due to the influence of relatively large amounts of detrital (volcanic fragment) content, but also because of a probable uranium leaching process (Ortega et al., 2005; Lachniet et al., 2012). Considering the stratigraphic relationships of tufa deposits as well as the ages obtained for upstream fluvial travertines, the same age range for these deposits should be expected.

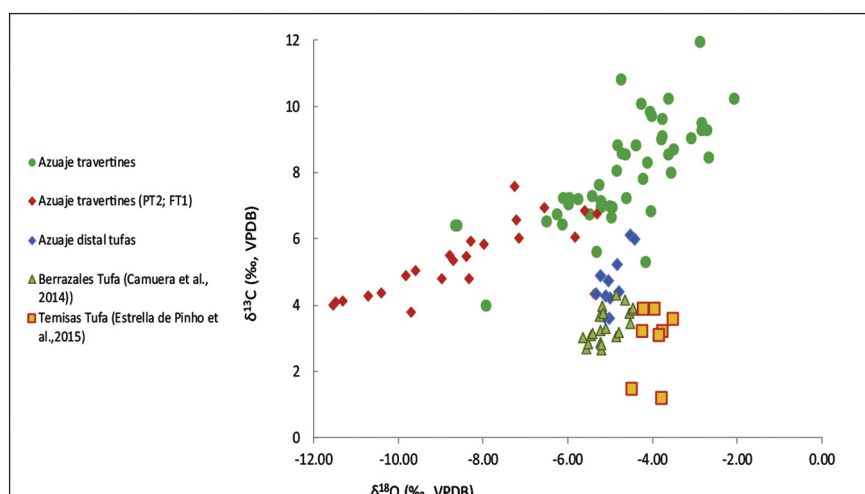


**Fig. 13.** Stable isotopes from Azuaje travertines and tufas; red rhombs correspond to outcrops PT2 and FT1, whereas green points correspond to the rest of travertines. Stable isotopes from Berrazales (Camuera et al., 2014), and Temisas (Estrella de Pinho et al., 2015), tufa deposits are represented for comparison.

## 5. Interpretation

### 5.1. Azuaje carbonate system

Azuaje carbonate system consists of both Holocene perched travertines with a fossil perched spring-line, and fluvial travertines, as well as fluvial tufas downstream from the travertines. Facies from Azuaje travertines and tufas reflect different sub-environments including pools, barriers, cascades and generally small waterfalls, channels and marginal (paludal) areas, as well as a wide range of sedimentary conditions related to flow velocity, water depth, and supersaturation in  $\text{CaCO}_3$  (Arenas-Abad et al., 2010; Jones and Renaut, 2010; Gandin and Capezzuoli, 2014). The erosive surface of lava and the clastic deposits at the base of fluvial carbonates strongly suggest that an erosive period occurred after lava emplacement and before the onset of fluvial carbonate sedimentation.

Although positive in both cases,  $\delta^{13}\text{C}$  values are higher in travertines than in tufas (Fig. 13) suggesting that the processes involved, mainly  $\text{CO}_2$  degassing were of higher magnitude in travertines.  $\delta^{13}\text{C}$  and  $\delta^{18}\text{O}$  values show wider ranges for travertines than for tufas, suggesting none to low re-equilibrium between DIC species as well as between DIC and  $\text{H}_2\text{O}$  for travertines than for tufas (Rodríguez-Berriguete et al., 2018). The presence of incompatible  $\text{Mn}^{2+}$  in aragonite, together with the small difference in  $\text{Sr}^{2+}$ ,  $\text{Ba}^{2+}$  and  $\text{Na}^{+}$  contents between aragonite

and calcite suggests that these cations were incorporated in aragonite and calcite structures with distribution coefficients different from those expected under equilibrium conditions, with precipitation occurring under disequilibrium conditions (Tesoriero and Pankow, 1996; Rimstidt et al., 1998; Dietzel et al., 2004; Day and Henderson, 2013). Decrease in  $\text{Mn}^{2+}$  and  $\text{Fe}^{2+}$  contents (Fig. 12; Table 1) of calcite from the perched travertines, close to springs, to distal fluvial tufas suggests that both oxidation and incorporation of these cations into calcite lattice mostly occur close to springs as has been reported by Pentecost (2005). Oppositely,  $\text{Mg}^{2+}$  contents seem to be very stable along the study area, suggesting that (i)  $\text{Mg}^{2+}$  contents in water were constant; and/or (ii) calcite precipitation rates were similar for travertines and tufas (Gabitov et al., 2014). However, as  $\text{CaCO}_3$  precipitates the  $\text{Mg}/\text{Ca}$  ratio and  $\text{Mg}$  contents in water should increase. Such increases would favour (i) a higher incorporation of  $\text{Mg}^{2+}$  into calcite lattice and (ii) aragonite precipitation in tufas, but none of them occurred. A higher precipitation rate in tufas may explain that, but it seems to be in contradiction with stable isotope data. A higher degree of hydration of  $\text{Mg}$  complexes in water, due to a slight increase in pH may explain a lower incorporation of  $\text{Mg}^{2+}$  in calcite referred to  $\text{Mg}^{2+}$  contents in water (Gabitov et al., 2014).

### 5.2. Facies associations in travertines

Travertine facies show changes, variations and alternations on a mm-scale, suggesting great sensitivity to changes in environmental conditions. An example is the oncoïd and stromatolite couple (Fig. 10A). Oncoïds form in relatively more energetic conditions, stirring available loose particles without impeding their microbial

**Table 2**  
 $\delta^{18}\text{O}$  and  $\delta^{13}\text{C}$  of the Azuaje travertines and tufas.

	$\delta^{18}\text{O}$ (‰V-PDB)				$\delta^{13}\text{C}$ (‰V-PDB)			
	Range	Max.	Mean	Min.	Range	Max.	Mean	Min.
All	9.47	−2.08	−5.72	−11.55	10.72	14.32	6.96	3.60
PT1, 2, 3	9.40	−2.15	−5.83	−11.55	10.54	14.32	7.25	3.78
PT1 & 3	3.97	−2.15	−3.97	−6.12	9.05	14.32	8.65	5.27
FT1, 2, 3	8.33	−2.08	−5.86	−10.41	6.42	10.78	7.51	4.36
FT2 & 3	6.58	−2.08	−5.26	−8.65	6.82	10.78	7.78	3.96
Distal tufa	0.90	−4.44	−4.95	−5.33	2.51	6.11	4.66	3.60
<i>Outcrops</i>								
PT1	3.87	−2.25	−4.29	−6.12	6.57	12.97	8.23	6.40
PT2	6.09	−5.39	−9.27	−11.48	2.13	5.91	4.77	3.78
PT3	2.00	−2.15	−3.29	−4.15	9.05	14.2	9.54	5.27
FT1	5.09	−5.31	−7.68	−10.41	3.22	7.58	6.13	4.36
FT2	6.58	−2.08	−4.97	−8.65	6.82	10.78	8.19	3.96
FT3	2.49	−4.02	−5.54	−6.50	3.16	9.67	7.37	6.51
T1	0.52	−4.81	−5.04	−5.33	1.62	5.22	4.29	3.60

**Table 3**  
 $^{87}\text{Sr}/^{86}\text{Sr}$  values for travertines and tufas of Azuaje.

Outcrop	Sample	$^{87}\text{Sr}/^{86}\text{Sr}$
PT1	COATEDGR	0.703628
	AZ-13A	0.703597
	AZ-16	0.703361
PT2	AZU6-7A	0.703565
	AZU-6B	0.703471
PT3	AZU1-1	0.703765
FT2	PRE-4A	0.703587
FT3	HOR-10	0.703483
T1	HOR-12B	0.703472
	Max.	0.703765
	Mean	0.703548
	Min.	0.703361

**Table 4**

U/Th datings of perched and fluvial travertines of Azuaje Ravine.

Outcrop	Sample	U-238 (ppm)	Th-232 (ppm)	U-234/U-238	Th-230/Th-232	Th-230/U-234	Nominal date (kiloyears BP)
PT1	POZ - 1	54.78	0.44	1.42 ± 0.01	18.409 ± 1.839	0.03 ± 0.00	3.70 ± 0.39
PT2	AZ - 16	4.02	0.02	5.30 ± 0.03	113.780 ± 18.140	0.03 ± 0.00	3.20 ± 0.11
PT2	AZU5-4	3.67	0.03	5.48 ± 0.04	58.557 ± 7.843	0.03 ± 0.00	3.01 ± 0.12
PT3	AZU - 6	14.13	0.09	2.48 ± 0.02	36.242 ± 2.998	0.03 ± 0.00	3.44 ± 0.20
FT2	AZU1-1	5.87	0.04	2.57 ± 0.03	34.053 ± 3.424	0.03 ± 0.00	2.89 ± 0.14
FT3	PRE - 3	5.64	0.02	2.89 ± 0.02	75.825 ± 7.100	0.03 ± 0.00	3.31 ± 0.13
FT3	PRE - 10	9.34	0.06	3.18 ± 0.02	41.936 ± 2.856	0.03 ± 0.00	3.17 ± 0.14

colonization, unlike those of stromatolite formation (Folk and Chafetz, 1983; Jones, 1991, 2009; Jones and Renaut, 1994; Maliva et al., 2000; Arenas-Abad et al., 2010; Gandin and Capezzuoli, 2014). Stromatolite formation occurs after previously formed oncoids become immobile and microbes colonize the surface on top of the oncoid accumulation (Jones and Renaut, 1994). Oncoid change into dendrites (Fig. 10B) instead of into stromatolites, occurs with a similar flow energy, but with a change from less supersaturated (oncoids) to more supersaturated waters (dendrites).

Interpretations of such changes or alternations between two facies can lead to more than one interpretation, as is the case of rafts becoming dendrites, both occurring under evaporative conditions (Gandin and Capezzuoli, 2014). First interpretation; there may be a change from stagnant to flowing waters under laminar regime, involving also a change from pool to terraced slope sub-environment. Second interpretation; there may be a change from relatively deeper water lamina to a very thin water film, both in shallow pool sub-environments (Jones and Renaut, 2010; Gandin and Capezzuoli, 2014), this latter case being the more probable interpretation.

A meaningful case deserving special attention is that of the facies changing from dendrites to stromatolites, or vice versa (Fig. 10C). Stromatolites form in a wide range of environmental conditions related to microbial colonization of fixed substrates (Schuster and Markx, 2014; Flemming et al., 2016). However, stromatolite formation can be interrupted and other facies can form, as for example, dendrites. This suggests that in some cases the environmental changes leading to the change from one facies to another surpass the limits tolerated by

microbes. In other words, some couples of facies such as stromatolite-dendrite, reflect a change in conditions from microbial-dominated to inorganic-dominated sedimentation (Fig. 14).

### 5.3. Facies associations in tufas

Couples of facies comprising loose particles (oncoids, intraclasts, etc.) becoming stromatolites vertically (Fig. 11B, C) can be interpreted as a result of a decreasing flow energy as in the case of travertines described above. However, the following questions should be considered. Unlike upstream travertines, tufa oncoids, intraclasts and phytoclasts accumulate as fluvial bedforms, such as bars in distal tufa deposits. Subsequent encrustation of the clastic mound or bar by stromatolite can be interpreted as a trend in decreasing water depth, reinforced by the common occurrence of hanging coated stems on the downstream side of the bar. Therefore, apparent changes in flow energy could be just the consequence of bedform evolution in a tractive fluvial regime.

On the other hand, repetition of mm-cm thick beds of oncoids (intraclasts, etc.) alternating with stromatolites suggests periodically repeated changes in flow energy, or changes from tractive (loose particle-dominated) to non-tractive (boundstone-dominated) fluvial regime. Repeatedly stacked horizontal beds or patches of palisades of coated vertical stems bounded by discontinuities (or becoming stromatolites on top) can be regarded as indicating a change from shallow fluvial or paludal to relatively deeper or more energetic fluvial environments. Repeated alternation between porous, thick and dense, thin stromatolitic lamination (Fig. 11A) has been attributed to changes

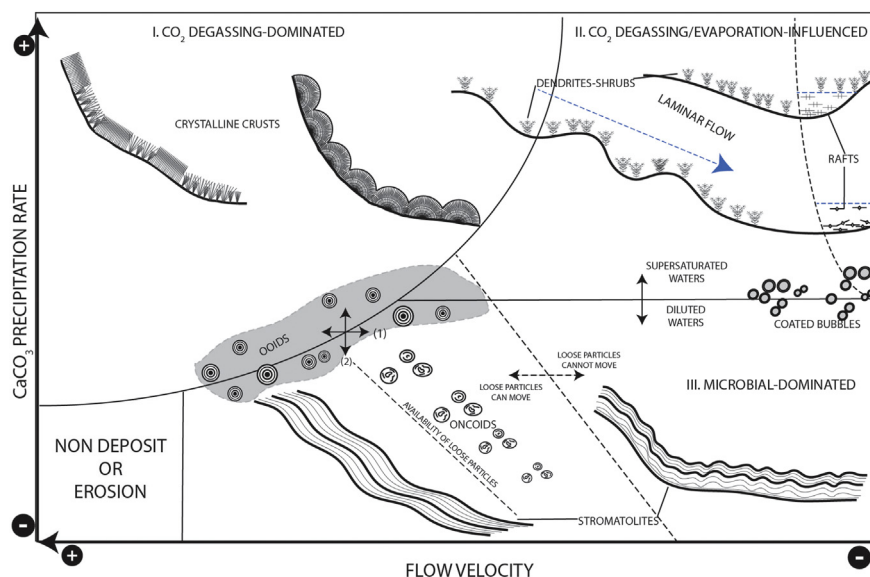


**Fig. 14.** Sketch showing the different travertine facies in relation to rate of calcium carbonate precipitation and velocity of current, factors related to abiogenic, biogenic and mixed processes. I. CO<sub>2</sub> degassing dominated field: flow velocity and/or CaCO<sub>3</sub> precipitation rate surpass microbial community toleration, with mostly abiotic precipitation. II. CO<sub>2</sub> degassing dominated-Evaporation-influenced field: flow velocity allows microbial colonization, but CaCO<sub>3</sub> precipitation rate surpasses microbial community toleration, so precipitation is dominantly abiotic. III. Microbial-dominated field: Flow velocity and precipitation rate do not surpass microbial colonization level, with sedimentation dominantly biotic-controlled or influenced. This sketch shows a wide range of situations within travertine-depositing systems, generally under very high precipitation rates. (1) Indicates conditions of low energy allowing microbial processes ( $V_{\text{flow}} < V_{\text{microbes}}$ ); (2) indicates precipitation rates lower than microbial growth rates ( $\text{CaCO}_3 \text{ precipitation rate} < \text{microbial growth}$ ).

in factors affecting sedimentation or  $\text{CaCO}_3$  precipitation rates, such as seasonal changes in  $\text{SI}_{\text{calcite}}$ , water temperature, or flow energy, among others (Kano et al., 2003; Liu et al., 2006, 2010; Okumura et al., 2012, 2013; Arenas et al., 2015). In summary, facies associations, changes and repetitions in Azuaje tufa deposits suggest periodic changes in flow energy and other parameters. However, care should be taken in the interpretation, as some of these changes can be due to sedimentary dynamics such as the formation of tractive bedforms.

## 6. Discussion

### 6.1. Facies associations in a travertine and distal tufa system: implications for sedimentary dynamics

Microbial colonization and biofilm development occur in a wide range of conditions (Schuster and Markx, 2014; Flemming et al., 2016), making microbial-related sedimentation potentially widespread. However, characteristic high  $\text{CaCO}_3$  precipitation rates and variable water regimes (flow velocity, water depth) in travertine and tufa-depositing systems, should be considered (Gradziński, 2010; Okumura et al., 2012; Arenas et al., 2015).

A  $\text{CaCO}_3$  precipitation rate exceeding the rate at which microbes maintain their position on the sedimentary surface where they develop biofilms, leads to dominant inorganic  $\text{CaCO}_3$  precipitation (Fields I and II in Fig. 14) (Gradziński, 2010; Schuster and Markx, 2014; Flemming et al., 2016). An example is the dendrite-stromatolite association, where dendrites grow at high rates impeding the thriving of microbes on top. Observations made by Jones (2017a; his Fig. 7A) and Peng and Jones (2013; their Fig. 2C, D), suggest that microbes are attached and restricted to uppermost dendrite branches but below the crystal growth front. Microbes only can colonize the sedimentary surface on top of previously formed dendrites when the crystal growth rate (and supersaturation) decreases below a certain level.

A flow velocity exceeding (i) the ability of microbes to attach to a substrate or (ii) the shear stress limit of a previously formed biofilm (Schuster and Markx, 2014; Flemming et al., 2016), leads to an absence of sedimentation (for sub-saturated waters) or to inorganic  $\text{CaCO}_3$  precipitation (for saturated-supersaturated waters) instead of microbial sedimentation (Field I in Fig. 14).

Many tufa, and some travertine facies associations reflect changes from relatively high (tractive) to low (non-tractive) flow energy. This suggests that flow energy was in some cases high enough to stir available loose particles, eventually becoming lower (Field III in Fig. 14), with clear microbial influence in both cases, suggesting appropriate conditions for microbes to thrive in both situations.

The changes in Azuaje travertines and tufas discussed above suggest conditions changing from (i) less to more evaporative (in travertines), (ii) more dilute to supersaturated (mainly in travertines; also, in tufas), and (iii) high to low energy (in travertines and tufas), all of them occurring within the same system. Most of these changes trend the same, suggesting similar environmental controls in both travertines and tufas (Liu et al., 2006, 2010; Okumura et al., 2012; Arenas et al., 2015).

Despite the similarity of environmental controls, some existing differences may strongly influence the formation of travertines and tufas. Some changes from perched and fluvial travertines to distal fluvial tufas include: (i) from aragonite-calcite to uniquely calcite compositions, (ii) decrease in  $\text{Mn}^{2+}$  and  $\text{Fe}^{2+}$  contents in calcite due to both incorporation in travertine calcite and oxidation, (iii) decrease in  $\delta^{13}\text{C}$  signal, and (iv) decrease in ranges of  $\delta^{13}\text{C}$  and  $\delta^{18}\text{O}$  values. Two important features remain unchanged from travertines to tufas: (i)  $\text{Mg}^{2+}$  content in calcite, and (ii)  $^{87}\text{Sr}/^{86}\text{Sr}$  ratio. The most commonly reported factors controlling formation of aragonite instead of calcite are high magnesium contents and  $\text{Mg}/\text{Ca}$  ratios, or strong  $\text{CO}_2$  degassing (Jones, 2017b and references therein). However, both  $\text{Mg}^{2+}$  contents and  $\text{Mg}/\text{Ca}$  ratios of water should increase from travertines to tufas as

aragonite and calcite precipitation progressed. Moreover, such increases would lead to higher magnesium contents in calcite and to aragonite formation (Fernández-Díaz et al., 1996; Jones, 2017b), none of them being observed in distal tufas. A slower dehydration or dehydroxylation rate of  $\text{Mg}$ -complexes in water may prevent a higher incorporation of  $\text{Mg}^{2+}$  into the calcite lattice and could be linked to a slight increase in pH (Gabitov et al., 2014) in spite of the possibly higher  $\text{Mg}^{2+}$  contents and  $\text{Mg}/\text{Ca}$  ratios as well as the probable lower  $\text{CaCO}_3$  precipitation rates in tufas compared to travertines. On the other hand, a decrease in  $\text{pCO}_2$  from travertines to tufas is also expected, as  $\text{CO}_2$  degassing progresses. Lower  $\text{CO}_2$  degassing rates may explain the lower  $\delta^{13}\text{C}$  signal of tufas compared to travertines. The lower ranges in both  $\delta^{13}\text{C}$  and  $\delta^{18}\text{O}$  values recorded in tufas also suggest higher degrees of re-equilibrium between DIC species as well as between DIC and water, probably linked to lower  $\text{CO}_2$  degassing rates and an increasing influence of biological photosynthetic activity than those occurring in travertines. Mixing of waters could also explain the change from travertine to tufa. Such mixing did take place as spring waters fell from ravine walls to the bottom. However,  $^{87}\text{Sr}/^{86}\text{Sr}$  ratios indicate that the origin of waters forming travertines and tufas is the same. This seems to be reinforced by the very low  $\text{Mn}^{2+}$  and  $\text{Fe}^{2+}$  contents of tufas, which are common close to springs (Pentecost, 2005) suggesting that there was not any spring close to the tufa deposits.

Successive vertical stacking of a couple of facies suggests periodic variations repeated throughout time. Although the precise periodicity of such variations cannot be easily assessed or generalized, most of these facies are compatible with seasonal cycles (Kano and Fujii, 2000; Kano et al., 2003; Liu et al., 2006, 2010; Gradziński, 2010; Arenas et al., 2015; Kovacs et al., 2018). This is the case of oncoid-stromatolite or phytoclast-raft associations, among others. In the case of our facies the system displays strong periodicity (seasonality?) with alternating humid/high flow energy to evaporative/low flow energy periods. This fits well with the current seasonality, with dry summers and torrential winter rainfalls (Marzol Jaén and Máyer Suárez, 2012; Mestre and Felipe, 2012).

On the other hand, facies such as dendrites can continue to grow regardless of seasonal or annual cycles, being commonly reported as polycyclic (Jones and Peng, 2016; Jones, 2017a). This suggests a certain stability in some sub-environments, probably due to stability of some springs in supplying water throughout the year.

In summary, variations in  $\text{CaCO}_3$  precipitation rates, and water flow energy related to microbial thriving, control the resulting travertine and tufa facies associations, providing information about sedimentary rhythms and trends in the system.

### 6.2. Travertines and tufas within the evolution history of the ravine and their relations with climate and hydrogeology

The presence of these travertines and tufas indicates that the piezometric level (water table) was higher than current one (Fig. 15) and the sedimentation rate surpassed the erosion rate during, at least 1.2 ka. The end of travertine deposition marks the drought of most of the springs (Fig. 15) and the onset of the erosive period until today (erosion > sedimentation) (Menéndez et al., 2008). It should be kept in mind that the erosive processes in this semi-arid setting are produced by few strong rainfalls throughout the year, exceeding 600 mm/year at headwaters of ravines (up 800–1000 m asl), helped by the high mean slopes of these ravines which may exceed 8% (Menéndez et al., 2008; Marzol Jaén and Máyer Suárez, 2012; Mestre and Felipe, 2012).

This lowering of the piezometric level, the drought of springs and the end of travertine deposition may be relevant for hydrogeology of the island, as seen in the Azuaje Ravine, one of the most deeply incised, with a very low bottom of the ravine altitude (Menéndez et al., 2008).

Ages of travertines of 3.7–2.9 ky BP indicate a period of carbonate deposition of about 1 ka after the end of the African Humid Period (AHP). The AHP caused a monsoonal-dominated climate during the Early to

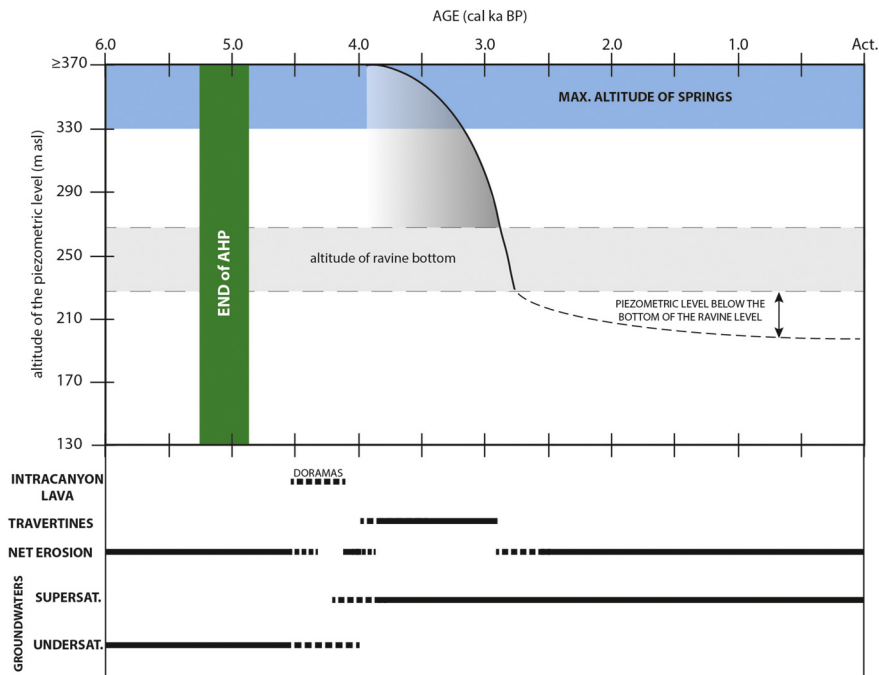


**Fig. 15.** Interpreted evolution (upper part) of piezometric level during the travertine-depositing period (continuous line), and at or after the end of sedimentation when piezometric level is below the bottom of the ravine. Evolution of the various geological processes occurred within this area of ravine since end of the African Humid Period to the present.

Mid-Holocene due to a more northwards Intertropical Convergence Zone (ITCZ) position than the current one. The end of the African Humid Period after 5.5–5.0 ky BP corresponded with a change from a monsoon-dominated, humid climate with rainfalls in summer to a more arid, trade wind-dominated climate with torrential rainfalls in winter (DeMenocal et al., 2000; Wanner et al., 2008; Vannière et al., 2011; Collins et al., 2013; Larrasoña et al., 2013; Enzel et al., 2015; Zielhofer et al., 2017a, 2017b), the latter being the current climate of the study area (Marzol Jaén and Máyer Suárez, 2012; Mestre and Felipe, 2012).

The onset of travertine deposition also corresponds with groundwater supersaturation, which also occurred after the AHP (Fig. 15). Groundwaters can be undersaturated if their residence time in the aquifer is not long enough (high aquifer discharge throughout springs, short residence times of groundwaters in the aquifer), or if there is a great input of waters to the aquifer (high aquifer recharge, short residence times of groundwaters in the aquifer) (Custodio, 2004; Kafri and Yechieli, 2010), to be expected during monsoon-dominated periods. A decrease in aquifer recharge (lower rainfall amount/infiltration) could change the situation to progressively more concentrated groundwaters, leading after some point to travertine deposition within the ravine. The end of travertine deposition marks the fall of the water table below the height of the bottom of the ravine (Fig. 15), but groundwaters of the area are still supersaturated (Hernández-Quesada, 2016; Rodríguez-Berriguete et al., 2018).

This places travertine and tufa deposition within a narrow time range where both high piezometric level and highly saturated groundwaters occurred after the end of the AHP (Fig. 15), so that carbonate deposition began with the lowering of water table of the island.

## 7. Conclusions

Travertines and tufas from Azuaje Ravine formation was related to aquifer evolution after Mid-Holocene climate change, but unrelated to neither active tectonics nor volcanism. Therefore, formation of these deposits should have been controlled uniquely by factors such as climate and hydrogeology, reflected in facies relationships. These

reflect periodic changes in flow velocity (or energy), water depth, or saturation state of the water throughout the whole system.

Conditions during travertine deposition comprise those allowing microbial-dominated facies (stromatolite), but also those leading to (mostly) inorganic precipitation (crystalline crusts, dendrites/shrubs) due to inhibition or strong limitation of microbial development on fixed substrates by the flow velocity and/or precipitation rate exceeding thresholds. Periodic and repeated changes from conditions alternately favouring or impeding microbial control are common.

Conditions during tufa deposition comprise those favouring deposition of microbially-dominated facies (stromatolites, coated stems) on fixed substrates, but also those indicating tractive conditions leading to transport, sedimentation and oncolitization of loose particles. Microbial-dominated facies developed on moving loose particles indicate that sedimentation was strongly microbially influenced under both tractive and non-tractive fluvial regimes, and conditions exceeding thresholds tolerated by microbes were uncommon.

The change from travertine to tufa may be due to decreases in aragonite and calcite supersaturations (and then in precipitation rates), CO<sub>2</sub> degassing rates, water temperatures, and probably pH and to microbial influence. All these changes are reflected in the mineralogy and geochemistry of travertines and tufas.

## Acknowledgements

This work was funded by project CGL2014-54818-P from the Spanish Ministerio de Ciencia e Innovación. J. Cerne reviewed the English version of the manuscript. Special thanks to A. Meléndez, F.J. Pérez-Torrado and M.C. Cabrera for their field assistance. M. Gradziński, B. Jones and an anonymous reviewer greatly helped to improve the original manuscript.

## References

- Abratis, M., Schmincke, H.U., Hansteen, T., 2002. Composition and evolution of submarine volcanic rocks from the central and western Canary Islands. *International Journal of Earth Sciences* 91 (4), 562–582.
- Arenas, C., Auqué, L., Osácar, C., Sancho, C., Lozano, M.V., Vázquez-Urbez, M., Pardo, G., 2015. Current tufa sedimentation in a high discharge river: a comparison with

- other synchronous tufa records in the Iberian Range (Spain). *Sedimentary Geology* 325, 132–157.
- Arenas-Abad, C., Vázquez-Urbez, M., Pardo-Tirapu, G., Sancho-Marcén, C., 2010. Chapter 3: Fluvial and associated carbonate deposits. In: Alonso-Zarza, A.M., Tanner, L.H. (Eds.), *Carbonates in Continental Settings: Facies, Environments and Processes*. Developments in Sedimentology 61, pp. 133–175.
- Aulinas, M., Gimeno, D., Fernandez-Turiel, J.L., Perez-Torrado, F.J., Rodriguez-Gonzalez, A., Gasperini, D., 2010. The Plio-Quaternary magmatic feeding system beneath Gran Canaria (Canary Islands, Spain): constraints from thermobarometric studies. *Journal of the Geological Society* 167 (4), 785–801.
- Balcells, R., Barrera, J.L., Gómez, J.A., 1992. Mapa Geológico de España a escala 1: 100,000 Gran Canaria. Instituto Tecnológico y Geominero de España (ITGE), Madrid.
- Camuera, J., Alonso-Zarza, A.M., Rodríguez-Berriguete, A., Rodríguez-González, A., 2014. Origin and palaeo-environmental significance of the Berrazales carbonate spring deposit, North of Gran Canaria Island, Spain. *Sedimentary Geology* 308, 32–43.
- Capezzuoli, E., Gandin, A., Pedley, M., 2014. Decoding tufa and travertine (freshwater carbonates) in the sedimentary record: the state of the art. *Sedimentology* 61 (1), 1–21.
- Carracedo, J.C., Perez-Torrado, F.J., Rodríguez Badiola, E., 2008. Canarias: islas volcánicas intraplaca. *GEOGUIAS VII Congreso Geológico de España*.
- Collins, J.A., Govin, A., Mulitza, S., Heslop, D., Zabel, M., Hartmann, J., Röhl, U., Wefer, G., 2013. Abrupt shifts of the Sahara-Sahel boundary during Heinrich stadials. *Climate of the Past* 9 (3), 1181–1191.
- Cousens, B.L., Spera, F.J., Tilton, G.R., 1990. Isotopic patterns in silicic ignimbrites and lava flows of the Mogan and lower Fataga Formations, Gran Canaria, Canary Islands: temporal changes in mantle source composition. *Earth and Planetary Science Letters* 96 (3–4), 319–335.
- Custodio, E., 2004. Hydrogeology of volcanic rocks. *Hydrogeology of Volcanic Rocks*. UNESCO, Paris, pp. 395–425.
- Day, C.C., Henderson, G.M., 2013. Controls on trace-element partitioning in cave-analogue calcite. *Geochimica et Cosmochimica Acta* 120, 612–627.
- DeMenocal, P., Ortiz, J., Guilderson, T., Sarnthein, M., 2000. Coherent high- and low-latitude climate variability during the Holocene warm period. *Science* 288 (5474), 2198–2202.
- Dietzel, M., Gussone, N., Eisenhauer, A., 2004. Co-precipitation of  $\text{Sr}^{2+}$  and  $\text{Ba}^{2+}$  with aragonite by membrane diffusion of  $\text{CO}_2$  between 10 and 50 °C. *Chemical Geology* 203 (1), 139–151.
- Enzel, Y., Kushnir, Y., Quade, J., 2015. The middle Holocene climatic records from Arabia: reassessing lacustrine environments, shift of ITCZ in Arabian Sea, and impacts of the southwest Indian and African monsoons. *Global and Planetary Change* 129, 69–91.
- Estrella de Pinho, R.R., Rodríguez-Berriguete, Á., Alonso-Zarza, A.M., Cabrera, M.C., 2015. The Temisas carbonate building: an example of thermogene tufa system in Gran Canaria Island. *Geogaceta* 57, 7–10.
- Fernández-Díaz, L., Putnis, A., Prieto, M., Putnis, C.V., 1996. The role of magnesium in the crystallization of calcite and aragonite in a porous medium. *Journal of Sedimentary Research* 66 (3), 482–491.
- Flemming, H.C., Wingender, J., Szewzyk, U., Steinberg, P., Rice, S.A., Kjelleberg, S., 2016. Biofilms: an emergent form of bacterial life. *Nature Reviews Microbiology* 14 (9), 563.
- Folk, R.L., Chafetz, H.S., 1983. Pisoliths (pisoids) in Quaternary travertines of Tivoli, Italy. *Coated Grains*. Springer, Berlin Heidelberg, pp. 474–487.
- Gabitov, R., Sadekov, A., Leinweber, A., 2014. Crystal growth rate effect on Mg/Ca and Sr/Ca partitioning between calcite and fluid: an in situ approach. *Chemical Geology* 367, 70–82.
- Gandin, A., Capezzuoli, E., 2014. Travertine: distinctive depositional fabrics of carbonates from thermal spring systems. *Sedimentology* 61 (1), 264–290.
- Gradziński, M., 2010. Factors Controlling Growth of Modern Tufa: Results of a Field Experiment. 336. Geological Society, London, pp. 143–191 (1). Special Publications.
- Gysi, A.P., Stefánsson, A., 2012. Mineralogical aspects of  $\text{CO}_2$  sequestration during hydrothermal basalt alteration—an experimental study at 75 to 250 °C and elevated  $\text{pCO}_2$ . *Chemical Geology* 306, 146–159.
- Hansteen, T.H., Troll, V.R., 2003. Oxygen isotope composition of xenoliths from the oceanic crust and volcanic edifice beneath Gran Canaria (Canary Islands): consequences for crustal contamination of ascending magmas. *Chemical Geology* 193 (3–4), 181–193.
- Hernández-Quesada, M., 2016. Funcionamiento hidrogeológico del área de los barrancos de Moya y Azuaje, norte de Gran Canaria (Doctoral dissertation).
- Jones, B., 1991. Genesis of terrestrial oncoids, Cayman Islands, British West Indies. *Canadian Journal of Earth Sciences* 28 (3), 382–397.
- Jones, B., 2009. Cave pearls—the integrated product of abiogenic and biogenic processes. *Journal of Sedimentary Research* 79 (9), 689–710.
- Jones, B., 2017a. Review of aragonite and calcite crystal morphogenesis in thermal spring systems. *Sedimentary Geology* 354, 9–23.
- Jones, B., 2017b. Review of calcium carbonate polymorph precipitation in spring systems. *Sedimentary Geology* 353, 64–75.
- Jones, B., Peng, X., 2016. Mineralogical, crystallographic, and isotopic constraints on the precipitation of aragonite and calcite at Shiqiang and other hot springs in Yunnan Province, China. *Sedimentary Geology* 345, 103–125.
- Jones, B., Renaut, R.W., 1994. Crystal fabrics and microbiota in large pisoliths from Laguna Pastos Grandes, Bolivia. *Sedimentology* 41 (6), 1171–1202.
- Jones, B., Renaut, R.W., 2010. Calcareous spring deposits in continental settings. In: Alonso-Zarza, A.M., Tanner, L.H. (Eds.), *Carbonates in Continental Settings: Facies Environments and Processes*. Elsevier, Amsterdam, pp. 177–224.
- Kafri, U., Yechieli, Y., 2010. Groundwater Base Level Changes and Adjoining Hydrological Systems. Springer Science & Business Media.
- Kano, A., Fujii, H., 2000. Origin of the gross morphology and internal texture of tufas of Shirokawa Town, Ehime Prefecture, Southwest Japan. *The Journal of the Geological Society of Japan* 106 (6), 397–412.
- Kano, A., Matsuoka, J., Kojo, T., Fujii, H., 2003. Origin of annual laminations in tufa deposits, southwest Japan. *Palaeogeography, Palaeoclimatology, Palaeoecology* 191 (2), 243–262.
- Kovacs, S.E., Reinhardt, E.G., Werner, C., Kim, S.T., Devos, F., Le Maillot, C., 2018. Seasonal trends in calcite-raft precipitation from cenotes Rainbow, Feno and Monkey Dust, Quintana Roo, Mexico: implications for paleoenvironmental studies. *Palaeogeography, Palaeoclimatology, Palaeoecology* 497, 157–167.
- Lachniet, M.S., Bernal, J.P., Asmerom, Y., Polyak, V., 2012. Uranium loss and aragonite–calcite age discordance in a calcitized aragonite stalagmite. *Quaternary Geochronology* 14, 26–37.
- Larrasoana, J.C., Roberts, A.P., Rohling, E.J., 2013. Dynamics of green Sahara periods and their role in hominin evolution. *PLoS One* 8 (10), e76514.
- Liu, Z., Li, H., You, C., Wan, N., Sun, H., 2006. Thickness and stable isotopic characteristics of modern seasonal climate-controlled sub-annual travertine laminae in a travertine-depositing stream at Baishuitai, SW China: implications for paleoclimate reconstruction. *Environmental Geology* 51 (2), 257–265.
- Liu, Z., Sun, H., Baoying, L., Xiangling, L., Wenbing, Y., Cheng, Z., 2010. Wet-dry seasonal variations of hydrochemistry and carbonate precipitation rates in a travertine-depositing canal at Baishuitai, Yunnan, SW China: implications for the formation of biannual laminae in travertine and for climatic reconstruction. *Chemical Geology* 273 (3–4), 258–266.
- Maliva, R.G., Missimer, T.M., Leo, K.C., Statom, R.A., Dupraz, C., Lynn, M., Dickson, J.A.D., 2000. Unusual calcite stromatolites and pisoids from a landfill leachate collection system. *Geology* 28 (10), 931–934.
- Marzol Jaén, M.V., MAYER Suárez, P., 2012. Algunas reflexiones acerca del clima de las islas Canarias. *Nimbus* 29–30.
- Menéndez, I., Silva, P.G., Martín-Betancor, M., Pérez-Torrado, F.J., Guillou, H., Scaillet, S., 2008. Fluvial dissection, isostatic uplift, and geomorphological evolution of volcanic islands (Gran Canaria, Canary Islands, Spain). *Geomorphology* 102 (1), 189–203.
- Mestre, A., Felipe, L., 2012. Atlas climático de los archipiélagos de Canarias, Madeira y Azores. Temperatura del aire y precipitación (1971–2000). Agencia estatal de Meteorología e Instituto de Meteorología de Portugal, Lisboa.
- Okumura, T., Takashima, C., Shiraishi, F., Nishida, S., Yukimura, K., Naganuma, T., Koike, H., Arp, G., Kano, A., 2011. Microbial processes forming daily lamination in an aragonite travertine, Nagano-yu Hot Spring, Southwest Japan. *Geomicrobiology Journal* 28 (2), 135–148.
- Okumura, T., Takashima, C., Shiraishi, F., Akmaluddin, Kano, A., 2012. Textural transition in an aragonite travertine formed under various flow conditions at Pancuran Pitu, Central Java, Indonesia. *Sedimentary Geology* 265, 195–209.
- Okumura, T., Takashima, C., Shiraishi, F., Nishida, S., Kano, A., 2013. Processes forming daily lamination in a microbe-rich travertine under low flow condition at the Nagano-yu Hot Spring, southwestern Japan. *Geomicrobiology Journal* 30 (10), 910–927.
- Ortega, R., Maire, R., Devès, G., Quinif, Y., 2005. High-resolution mapping of uranium and other trace elements in recrystallized aragonite–calcite speleothems from caves in the Pyrenees (France): implication for U-series dating. *Earth and Planetary Science Letters* 237 (3–4), 911–923.
- Ovchinnikova, G.V., Belyatskii, B.V., Vasil'eva, I.M., Levskii, L.K., Grachev, A.F., Arana, V., Mithavila, J., 1995. Sr–Nd–Pb isotope characteristics of the mantle sources of basalts from the Canary Islands. *Petrology* 3 (2), 172–182.
- Özkul, M., Varol, B., Alçiçek, M.C., 2002. Depositional environments and petrography of Denizli travertines. *Bulletin of the Mineral Research and Exploration* 125, 13–29.
- Peng, X., Jones, B., 2013. Patterns of biomediated  $\text{CaCO}_3$  crystal bushes in hot spring deposits. *Sedimentary Geology* 294, 105–117.
- Pentecost, A., 2005. *Travertine*. Springer, Berlin (445 pp.).
- Pérez-Torrado, F.J., Carracedo, J.C., Mangas, J., 1995. Geochronology and stratigraphy of the Roque Nublo Cycle, Gran Canaria, Canary Islands. *Journal of the Geological Society* 152 (5), 807–818.
- Pirajno, F., 2009. *Hydrothermal Processes and Mineral Systems*. Springer, Netherlands (1250 pp.).
- Rimstidt, J.D., Balog, A., Webb, J., 1998. Distribution of trace elements between carbonate minerals and aqueous solutions. *Geochimica et Cosmochimica Acta* 11, 1851–1863.
- Rodríguez Berriguete, Á., 2017. Petrología, sedimentología y geoquímica de los travertinos y tobas del Barranco de Azuaje (Gran Canaria): características e implicaciones. (Doctoral dissertation). Universidad Complutense de Madrid.
- Rodríguez-Berriguete, Á., Alonso-Zarza, A.M., Cabrera, M.C., Rodríguez-González, A., 2012. The Azuaje travertine: an example of aragonite deposition in a recent volcanic setting, N Gran Canaria Island, Spain. *Sedimentary Geology* 277–278, 61–71.
- Rodríguez-Berriguete, Á., Alonso-Zarza, A.M., Martín-García, R., Cabrera, M.C., 2018. Sedimentology and geochemistry of a human-induced tufa deposit: implications for palaeoclimatic research. *Sedimentology* 65, 2253–2277.
- Rodríguez-Gonzalez, A., Fernandez-Turiel, J.L., Perez-Torrado, F.J., Hansen, A., Aulinas, M., Carracedo, J.C., Jimeno, D., Guillou, H., Paris, R., Paterné, M., 2009. The Holocene volcanic history of Gran Canaria island: implications for volcanic hazards. *Journal of Quaternary Science* 24 (7), 697–709.
- Schuster, J.J., Marx, G.H., 2014. Biofilm architecture. *Productive Biofilms*. Springer, Cham, pp. 77–96.
- Shiraishi, F., Eno, Y., Nakamura, Y., Hanzawa, Y., Asada, J., Bahniuk, A.M., 2018. Relative influence of biotic and abiotic processes on travertine fabrics, Satono-yu hot spring, Japan. *Sedimentology* 66 (1).
- SPA–15, 1975. Estudio científico de los recursos de agua en las Islas Canarias (SPA/69/515). Ministerio de Obras Públicas. Dirección General de Obras Hidráulicas. UNESCO, Las Palmas de Gran Canaria, España.
- Stefánsson, A., Sveinbjörnsdóttir, Á.E., Heinemeier, J., Arnórsson, S., Kjartansdóttir, R., Kristmannsdóttir, H., 2016. Mantle  $\text{CO}_2$  degassing through the Icelandic crust:

- evidence from carbon isotopes in groundwater. *Geochimica et Cosmochimica Acta* 191, 300–319.
- Tesoriero, A.J., Pankow, J.F., 1996. Solid solution partitioning of  $\text{Sr}^{2+}$ ,  $\text{Ba}^{2+}$ , and  $\text{Cd}^{2+}$  to calcite. *Geochimica et Cosmochimica Acta* 60 (6), 1053–1063.
- Thirlwall, M.F., Jenkins, C., Vroon, P.Z., Matthey, D.P., 1997. Crustal interaction during construction of ocean islands: Pb-Sr-Nd-O isotope geochemistry of the shield basalts of Gran Canaria, Canary Islands. *Chemical Geology* 135 (3), 233–262.
- Vannière, B., Power, M.J., Roberts, N., Tinner, W., Carrión, J., Magny, M., Bartlein, P., Colombaroli, D., Daniau, A.L., Finsinger, W., Gil-Romera, G., Kaltenrieder, P., Pini, R., Sadori, L., Turner, R., Valsecchi, V., Vescovi, E., 2011. Circum-Mediterranean fire activity and climate changes during the mid-Holocene environmental transition (8500–2500 cal. BP). *The Holocene* 21 (1), 53–73.
- Wanner, H., Beer, J., Bütikofer, J., Crowley, T.J., Cubasch, U., Flückiger, J., Goosse, H., Grosjean, M., Joos, F., Kaplan, J.O., Küttel, M., Müller, S.A., Prentice, I.C., Solomina, O., Syöcker, T.F., Tarasov, P., Wagner, M., Widmann, M., 2008. Mid-to Late Holocene climate change: an overview. *Quaternary Science Reviews* 27 (19), 1791–1828.
- Zielhofer, C., von Suchodoletz, H., Fletcher, W.J., Schneider, B., Dietze, E., Schlegel, M., Schepanski, K., Weninger, B., Mischke, S., Mikdad, A., 2017a. Millennial-scale fluctuations in Saharan dust supply across the decline of the African Humid Period. *Quaternary Science Reviews* 171, 119–135.
- Zielhofer, C., Fletcher, W.J., Mischke, S., De Batist, M., Campbell, J.F., Joannin, S., Tjallingii, R., El Hamouti, N., Junginger, A., Stele, A., Bussmann, J., Schneider, B., Lauer, T., Spitzer, K., Strupler, M., Brachert, T., Mikdad, A., 2017b. Atlantic forcing of Western Mediterranean winter rain minima during the last 12,000 years. *Quaternary Science Reviews* 157, 29–51.